INTERACTIONS OF CADMIUM SELENIDE (CdSe) QUANTUM DOTS WITH COAGULANT PROTEINS EXTRACTED FROM *MORINGA OLEIFERA* SEEDS

A MINI THESIS SUBMITTED IN PARTIAL FULFILMENT

OF THE REQUIREMENTS FOR THE DEGREE

OF

MASTER OF SCIENCE IN CHEMISTRY

OF

THE UNIVERSITY OF NAMIBIA

BY

SALATIEL KAPOFI

200937545

March 2019

SUPERVISOR: Prof HABAUKA KWAAMBWA *(Department of Natural and Applied Sciences, Namibia University of Science and Technology)*

CO-SUPERVISOR: Dr. LIKIUS DANIEL *(Department of Chemistry and Biochemistry, University of Namibia)*

CO-SUPERVISOR: Prof MARTHA KANDAWA-SCHULZ *(Department of Chemistry and Biochemistry, University of Namibia)*

ABSTRACT

In order to investigate the interaction mechanism between Cadmium selenide (CdSe) quantum dots (QDs) and *Moringa oleifera* seeds coagulant protein (MOCP), CdSe QDs with hexagonal phase and crystalline size of 3.1-8.1 nm were synthesized in presence of organic solvent Trioctyl-n-phosphine oxide (TOPO) and Trioctyl phosphene (TOP) using colloidal synthesis. The purified mesoporous *M. oleifera* seeds coagulant protein (MOCP) with a surface area of 8.4134 m^2/g, was extracted from *M. oleifera* seeds. The interaction mechanism between CdSe QDs and MOCP was studied using the Ultraviolet (UV)-vis absorption spectroscopy, fluorescence (FL) emission spectroscopy and the Fourier Transform Infrared spectroscopy (FTIR). The UV-vis absorption spectrum showed an absorption band of CdSe and MOCP at 546.5 nm, with an increase in concentration of MOCP the absorbance intensity decreased. This shows the molecular complexation between CdSe QDs and MOCP in formation of CdSe-MOCP complex. The FL spectroscopy revealed the excitation wavelength of MOCP and CdSe QDs at 302.7 nm and 602.4 nm respectively. The FL intensity of CdSe QDs was found to decrease with an increasing concentration of MOCP, as such it was classified as static quenching mechanisms. Using Stern-Volmer analysis, the binding constants (K_b), quenching constants (K_q) and number of binding sites (n) were determined. The thermodynamic potentials ΔH^{θ}(-321.3 $kJmol^{-1}$); ΔS^{θ}(156.0 $JK^{-1}mol^{-1}$) and ΔG^{θ}(-46.6 $kJmol^{-1}$) were calculated and gave an indication that the interaction is a results of the electrostatic interactions, hydrophobic and van der waal forces. The stable CdSe-MOCP complex is said to be formed as a results of CdSe QDs adsorbed onto MOCP through electrostatics interaction and surface bound complexation equilibrium attraction. The CdSe-MOCP can be studied for application in water treatment, labeling agent and as sensors.

Table of Contents

LIST OF TABLES

LIST OF FIGURES

LIST OF ABBREVIATIONS AND/OR ACRONYMS

AFP	Alpha-Fetoprotein Antibody
Au-NPs	Gold Nanoparticles
BET	Brunaver-Emmett-Teller
BOI	Biomolecules
BSA	Boxin Serum Albumin
CdSe-ZnS	Cadmium Selenide Zinc Sulfide
CdSe-MOCP	Cadmium Selenide *Moringa Oleifera* Seeds Coagulant Protein
CdTe	Cadmium Telenide
CMC	Carboxyl methyl Cellulose
CTAB	Cetyltrimethylammonium
DDT	Dichlorodiphenyltrichloroethane
DHLA	Dihydrolipoic Acid
DNA	Deoxyribonucleic Acid
EDC	1-Ethyl-3-(3-dimethylaminopropyl) Carbodiimide
EDX/EDA	Energy Dispersive X-Ray Analyzer
FTIR	Fourier Transform Infrared Spectroscopy
Hb	Hemoglobin
HDA	Hexadecyl Amine
HRTEM	Higher Resolution Transmission Electron Microscopy
LED	Light Emitting Diode
LHE	Light Harvesting Efficiency
lnAs	Indium Arsenide
MAA	Mercapto Acetic Acid
MBP	Maltose Binding Protein

MEG	Multiple Exciton Generation
MOCP	*Moringa Oleifera* Seeds Coagulant Protein
MOP	*Moringa Oleifera* Protein
ONIOM	Our Own N-layered Integrated Molecular Orbital + Molecular Mechanics
PbSe	Lead Selenide
PEG	Polyethylene Glycol
QDs	Quantum dots
QM/MM	Quantum Mechanics/Molecular mechanics
SDBS	Sodium Dodecyl Benzene Sulfonate
SDS	Sodium dodecylsulfate
SEM	Scanning Electron Microscopy
TGA	Thioglycolic acid
TOP	Trioctylphosphine
TOPO	Trioctylphosphine Oxide
UV-Vis	Ultraviolet-Visible Spectroscopy
XRD	X-ray Powder Diffraction
ZnSe	Zinc Selenide

ACKNOWLEDGEMENTS

I would like to express my utmost appreciation and thanks to my supervisors **Prof Habauka Kwaambwa** and **Dr Daniel Likius** for accepting me under their trusted tutorage. They have constantly offered invaluable assistance, support and guidance positively from the beginning and toward the completion of my study. I also feel grateful for their innovative ideas, integrity and dedication toward my research project which has inspired me so much. Equivalently let me extend my profound gratitude to my co-supervisor **Prof Martha Kandawa-Schulz**, for she has been a driving force, providing emotional support and ensuring my success during the difficult time I have endured in pursuing this course.

It is genuine pleasure to express my deep sense of appreciation and thanks to my brother **Tate Frans Kapofi** and **Meme Nakutshe Kapofi**; for their encouragement, understanding, their endless support and love they equally offered during my study period. Thank you for your warm shoulder that I leaned on. I thank profusely my mother **Meme Saara Shangadi** for continual life coaching; your prayer for me is what sustained me thus far. Heartfelt gratitude to my fellow staff members (**David**, **John**, **Nande**, **Ndunge**, **Hilaria**) in the Department of Chemistry/Biochemistry, who have supported me, advised and offered me counselling during my study. Singular gratitude to **Mr. Simeon Hamukoshi** for assistance he offered in carrying out my measurements. I also would like to appreciate my Trio undergraduate team **Shipiki MO**, **Ndashivika JV** and **Ntinda MIS** for their endless and magnificent support that they equally offered upon my entire request, which created space for me to focus on my research. Thanks to my friends for their added value, their endless support in my academic needs and good influences that incented me to strive toward my goal.

I know that all was by you, **God**! Thank you.

DEDICATION

In my heart I plan, but God determined all my steps. Against this background, I would dearly dedicate this Thesis to God the glory. May his peace that surpasses all understanding govern and sustain our wellbeing.

DECLARATION

I, Salatiel Mweuhala Kapofi, hereby declare that this study is my own work and is a true reflection of my research and that this work or any part thereof has not been submitted for a degree at any other institution.

…… ……. ……..

Name of Student **Signature** **Date**

CHAPTER 1: INTRODUCTION

1 Background of the Study

Research has established that the aqueous or saline water proteins extracted from *Moringa oleifera* seeds are low molecular mass and have coagulation and flocculating properties for water treatment [1]. Many studies have focused mainly on the extraction and purification of the *M. oleifera* seeds protein for the efficiency and evaluation of the quality of treated water [2, 3]. Although it is generally accepted from numerous studies that the *M. oleifera* seeds possess a short protein chain with coagulating properties, this protein seems to differ depending on the extraction and purification methods used [4]. *M. oleifera* seeds protein is used as an alternative to the common coagulants such as aluminium salts, iron salts and synthetic polymers in water treatment. The latter coagulant agents are expensive and have negative environmental and health effects. For instance, aluminium salts have been associated with Alzheimer's disease [5]. Kwaambwa and Maikokera [6] conducted studies to understand the mechanism of water treatment by the *M. oleifera* seeds protein. In these studies, the number of peculiar physicochemical properties of the water purification protein from *M. oleifera* seeds have been determined which includes its resistance to pH in the range 4-9, ionic strength effect, adsorption to different surfaces and floc strength and floc dimension., However they have not been able to address fundamental concepts of *M. oleifera* seeds protein such as its charge characteristics Its number of binding sites was found to be 1.50, the binding constants was found to be in range 1.78 $x10^{-5}$ to 1.00 $x10^{-4}$. Due to the unique physicochemical properties of *M. oleifera* seeds protein, its interaction mechanisms with charged particles

are investigated, in the current study particularly by studying their interaction with Cadmium Selenide quantum dots (CdSe-QDs).

Quantum dots are considered to be a relatively new class of nano-materials made up of inorganic atoms coated with the organic layer. QDs gained interest and found application in various areas such as medicine, chemistry, biology and technology due to their unique electronic, optical and chemical properties [7]. Despite the remarkable studies done on these nanocrystals QDs, little is known about the surface modification and the interaction mechanism of nanoparticles with macromolecules [7, 8]. The surface modification of the quantum dots has a greater effect as it enhances their exciton properties and also boosts up the photo-stability of the semiconductor; In addition, the protein-quantum dots interactions was found to have an influence in the properties of protein and quantum dots alike such as bang gap, photostability, emission and absorption spectra [9,10]. The study reported by Galian and Guardia [11] supported that biomolecules particularly proteins can be labelled with QDs and the QDs-analyte interaction are classified into three categories; direct binding of the analyte to the QDs surface, electrostatic interaction and the host-guest chemistry on the QDs surface. The study of the interaction of *M. oleifera* seeds coagulant protein (MOCP) with CdSe QDs has not been reported, thus the MOCP will not just be used as a model protein in this study but also help further understanding of the colloidal and physicochemical properties of this natural protein.

This study employed the CdSe quantum dots interaction with *M. oleifera* seeds coagulant protein to investigate the properties of *M. oleifera* seeds protein through QDs-Protein

interactions namely the CdSe-MOP complex. The CdSe-MOP complexes were studied using different instrumentation such as Fluorescence (FL) spectroscopy, Fourier Transform Infrared spectroscopy (FTIR) and Ultraviolet-Visible (UV-Vis) spectroscopy. The current study has also characterized the CdSe, using nano-scale instruments such Scanning electron microscopy (SEM), Higher resolution transmission microscopy (HRTEM) and X-ray Powder Diffraction (XRD).

1.2 Statement of the problem

The interaction of QDs with biomolecules, particularly proteins such as haemoglobin, human serum albumin and many more, has attracted a lot of research [11, 12]. In spite of many studies on the interaction of QDs with biological molecules, more detailed investigations are necessary due to many factors that affect the interaction mechanisms such as the size, surface charge and structure of QDs [8, 10]. Interaction of QDs with the coagulant protein from *M. oleifera* has not been reported. This study investigated the interaction mechanisms between CdSe QDs and MOCP, which showed that the CdSe-MOCP complex is formed by means of molecular complexation, hydrophobic, van der Waals forces and that electrostatic interaction played the key role in the stabilization of CdSe-MOCP complex.

1.3 Objectives of the study

The objectives of this study are:

(a) To prepare and characterize the CdSe QDs and CdSe-MOCP complex.

(b) To investigate the mechanism of interaction between MOCP and CdSe QDs.

(c) To determine the physicochemical and colloidal properties of MOCP with QDs.

1.4 Significance of the study

The study investigated the colloidal and physicochemical properties of the natural protein of *M. oleifera* seeds extract. The data generated will be of greater value to the biophysical chemistry studies. The understanding of physical and chemical properties of *M. oleifera* seed proteins extract will provide new insights into their potential applications in water treatment and in other areas such as biomedical fields as sensors and labeling agents.

CHAPTER 2: LITERATURE REVIEW

2.1 Description of Quantum Dots

Colloidal Semiconductor nanoparticles quantum dots are also referred to as artificial atoms with dimension range from one to the tenth of a nanometer, and they are restricted in three dimensional to a quasi-spherical shape [13]. The study by Miguel and Guardia [14] reported that the semiconductor nanoparticles are synthesized from atoms comprising of alkyl metals, metal oxides, transition metals or organic salts coupled to group VI elements (Se, S and Te). They are often coated with an inorganic shell such as ZnS to enhance the stability and to lengthen the fluorescence quantum yield [7]. QDs are synthesized with organic ligand trioctylphosphine oxide (TOPO) and trioctylphosphine (TOP) which make them soluble in an organic solvent [14]. The prominent term in nanotechnology is the quantum confinement effect, which is a result of a change in the atomic structure of a material at the nanoscale [15].

Nanoparticles exhibit new unique properties as a result of quantum size confinement in nanocluster, with large surface to volume ratio than the bulk materials [16], and they display more pronounced properties in their electronic states and optical properties such as broad absorption spectra, narrow emission spectra, broadband exciton, high quantum yield, photo stability and readily tunable spectra [8, 17, 18]. These properties can be engineered to fit the needs of particular experiment, biological or technological application. As a result these attributes of QDs, captivated lot of research, thus in recent decades QDs have been applied in various fields, biological imagining and cell labeling [19], biomolecules detection [20], optoelectronic and solar energy, immune reaction

analysis [21], quantum computing [85], drug screening [22] and in many more technological areas.

The QDs CdSe and CdSe/ZnS are classified as type I and type II QDs, respectively due to the location of carriers, electron and hole. In type I QDs the electron and hole are confined in a core region, hence it enhance the radiative recombination and improve optical stability [25], In contrast, type II QDs have a staggered bandgap alignment which promotes spatial separation of electron and hole into different regions of the core/shell structures. CdSe is a core quantum dots and when its surface is modified through passivation with ZnS it becomes a core/shell type II quantum dots. (CdSe-ZnS QDs is a type II quantum dots which have an increased quantum yield, higher optical stability and have reduced biotoxicity as compared to CdSe QDs type I [26]. The difference between type I and type II is illustrated in Figure 1.

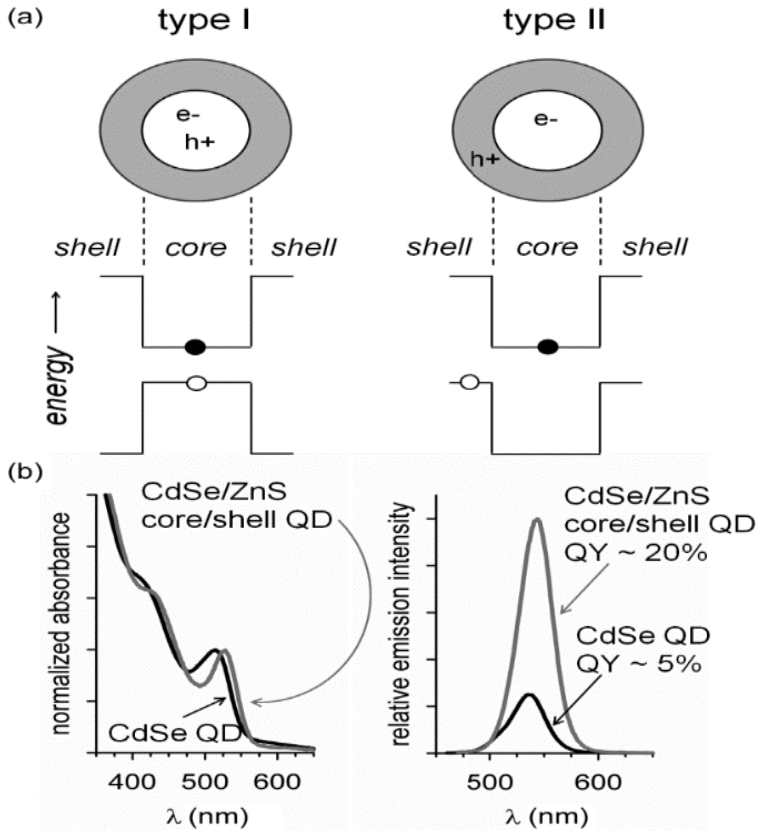

Figure 1: (a) Structure of electron and hole in type-I and type-II CdSe and CdSe/ZnS QDs. (b) represent the difference in optical properties of CdSe and CdSe/ZnS Quantum dots [27].

2.2 Quantum Confinement Effect in semiconductor nanoparticles

The quantum confinement effect in CdSe, (CdSe) ZnS and ZnS nanoparticles occurs in the length scale of mostly 1 to 10 nm, in which the spatial electronic wave function is said to be proportional to the particle size. The electrons in CdSe and (CdSe) ZnS QDs are restricted by the particle boundaries, thus the reduction of particle size influence the electrons to adapt by adjusting their energy [28]. This process is called quantum size effect. The quantization effect is said to be more pronounced when the dimension of particles is lower than the bulk semiconductor Bohr exciton radius. Bohr radius of the particle is defined as [29, 30]

$$a_b = \varepsilon_r \left(\frac{m}{\mu}\right) a_0 \ldots\ldots\ldots\ldots\ldots\ldots\ldots\ldots\ldots\ldots\ldots\ldots\ldots\ldots\ldots\ldots\ldots\ldots\ldots\ldots\ldots\ldots\ldots\ldots\ldots\ldots (1)$$

where ε_r is the dielect constant of material, m is the mass of electron, a_0 is the Bohr radius of hydrogen atom and μ is the mass of particle. The study by Onyia et al [31], demonstrated the concept of quantum box model in which the electron motion is bound to a three dimensional wall. This concept predicted that the Energy of band gap in a spherical QDs of radius (R) is proportional to $1/R^2$. Moreover, a deduction was drawn that as particles size of QDs decreases, the energy of band gap (E_g) increases.

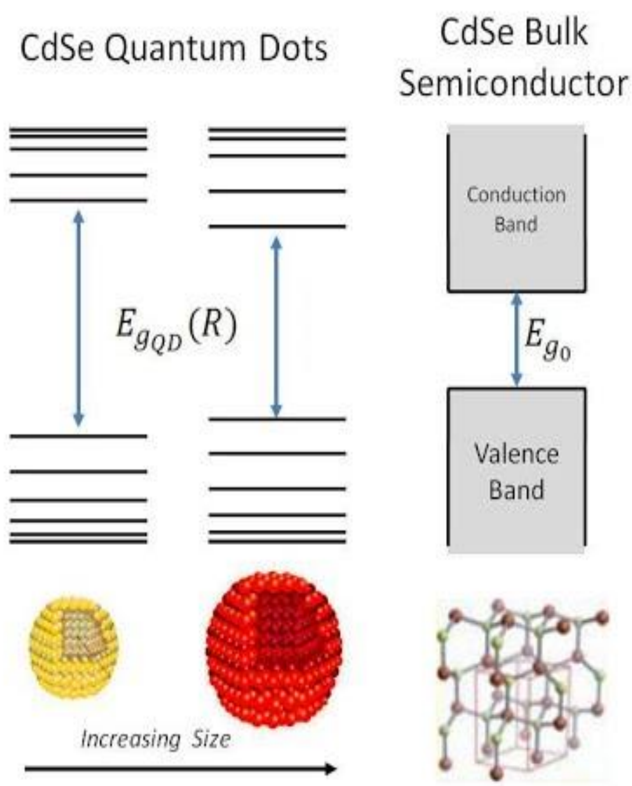

Figure 2: Demonstration of size-dependent band gap structure on the size of semiconductor materials [32].

Electrons exist at discrete energy levels known as bands in all material. When semiconductors nanoparticles materials such as CdSe, CdSe/ZnS, CdTe and ZnSe is

stricken by a photon, an electron transit from the valence band to the conduction band in the creation of electron/hole pair. The relaxation of the electron and hole is caused by a nonradiative process which leads to the loss of energy equal to the effective band gap of the dots which is emitted as light [33].

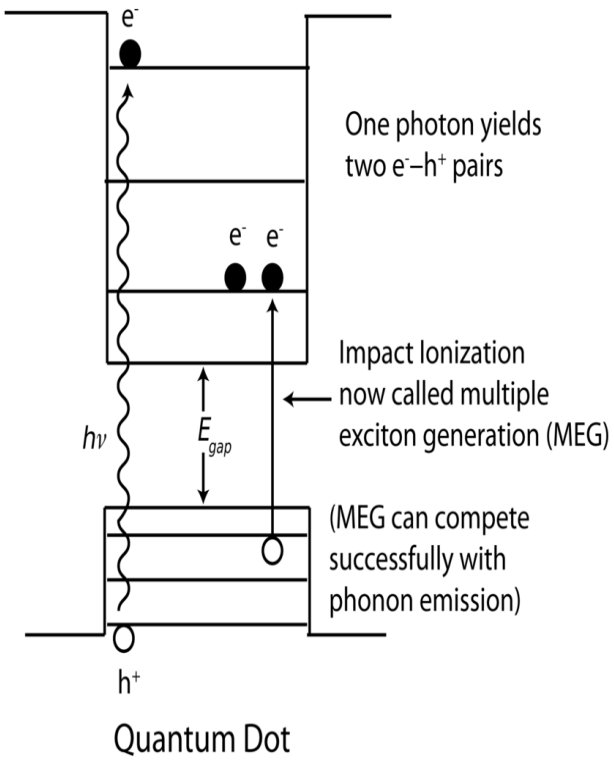

Figure 3: Multiple electron excitation processes [34], the input of energy, photon irradiation results into a generation of two electron carrier (e-- h+ pair). This process is referred to as multiple exciton generations (MEG) which is essential in the enhancement.

2.2.1 Theoretical Models

The quantum confined structure is described by the motion of carriers (electron/hole) which are confined in one or more directions by the potential barriers [35]. Depending on the direction of confinement, the confined quantum structure is categorized as quantum

well, quantum wire and quantum dots [36]. The quantum dots are zero-dimensional and the electron motions are confined in three dimensional. It's significant to specify the energy and eigenvalues of electrons and holes in a quantum dot, thus an approximation of an infinite potential is used, whereby the quantum dots is treated as a particle in the box model [37]. The Schrödinger equation [38] for electrons confined in one dimensional infinite square potential well is employed.

$$\frac{-\hbar^2}{2m}\frac{d^2\varphi_n}{dx^2} + V(x)\varphi_n = E_n\varphi_n \quad \ldots\ldots (2)$$

The Eigen-wave function $\varphi_n(r)$ and the energy values E_n of the Schrödinger equation are defined as follows:

$$\varphi_n(x) = \sqrt{\frac{2}{L}}\, sin\left(\frac{n\pi}{L}\, x\right) + \sqrt{\frac{2}{L}}\, cos\left(\frac{n\pi}{L}\, x\right) \quad \ldots\ldots (3)$$

$$E_n = \frac{\pi^2\hbar^2}{2mL^2}n^2, n = 1,2,3,4 \quad \ldots\ldots (4)$$

The energy of band gap is defined by:

$$E_g = E_{g0} + \frac{\hbar^2\pi^2}{2m_{eh}R^2} \quad \ldots\ldots (5)$$

$$m_{eh} = \frac{m_e m_h}{m_e + m_h} \quad \ldots\ldots (6)$$

Defining the variables m_{eh} is the effective mass of electron/hole pair; R is Bohr radius of quantum dots, E_{g0} is the band gap energy of bulk material (semiconductor) and E_g is the energy of the band gap of QDs.

According to the literature [39], the total energy of the Quantum dot is defined by:

$$E_{QD} = E_{band\ gap} + E_{confiment} + E_{excitation} \quad \ldots\ldots (7)$$

The total confinement energy, energy levels and energy of the carrier (holes or electrons) can be obtained by solving the Schrödinger equation.

$$\left(\frac{-\hbar^2}{2m}\left[\frac{\partial^2}{\partial x^2}+\frac{\partial^2}{\partial y^2}+\frac{\partial^2}{\partial z^2}\right]+V(x,y,z)\right)\varphi(x,y,z)=E\varphi(x,y,z) \ldots\ldots\ldots\ldots\ldots\ldots\ldots\ldots (8)$$

The quantum dots or nanocrystals are confined in three dimensional,

The energy of QDs is given by;

$$E_{n,m,l}=\frac{\pi^2\hbar^2}{2m}\left[\frac{n^2}{{L_x}^2}+\frac{m^2}{{L_y}^2}+\frac{l^2}{{L_Z}^2}\right]\varphi=\emptyset(x)\emptyset(y)\emptyset(z) \ldots\ldots\ldots\ldots\ldots\ldots\ldots\ldots\ldots\ldots\ldots\ldots\ldots (9)$$

The quantum wire is confined on only two dimensional,

The energy of Quantum wire is given by:

$$E_{n,m}(k_x)=\frac{\pi^2\hbar^2}{2m}\left[\frac{n^2}{{L_z}^2}+\frac{m^2}{{L_y}^2}\right]+\frac{\hbar^2{k_x}^2}{2m}\ \varphi=\phi(z)\phi(y)e^{ik_xx} \ldots\ldots\ldots\ldots\ldots\ldots\ldots\ldots\ldots (10)$$

The quantum well is confined in only one dimensional

The energy of Quantum well is given by:

$$E_n(k_xk_y)=\frac{\pi^2\hbar^2n^2}{2mL^2{}_Z}+\frac{\hbar^2}{2m}({k_x}^2{k_y}^2)\varphi=\phi(z)e^{(ik_x{}^2+ik_y{}^2)} \ldots\ldots\ldots\ldots\ldots\ldots\ldots\ldots\ldots\ldots (11)$$

Defining the parameters *n, m, l* =1, 2, 3….are the quantum confinement numbers, L_x, L_y, L_z are the confining dimensions and $e^{(ik_xx+ik_yy)}$ is the wave function describing the electronic motion in x and y direction.

The confinement energy and Excitation energy is obtained by solving the above Schrödinger equation and defined as follows:

$$E_{confiniment}=\frac{\hbar^2\pi^2}{2a^2}\left(\frac{1}{m_e}+\frac{1}{m_h}\right) \ldots\ldots\ldots\ldots\ldots\ldots\ldots\ldots\ldots\ldots\ldots\ldots\ldots\ldots\ldots\ldots\ldots\ldots\ldots\ldots (12)$$

The energy level in QDs are discrete and their bandgap is said to be always energetically larger; thus the radiation from QDs is referred to as “blue shifted”. Radiation is a result

of electrons excitation from one energy level to the excited state, the difference in energies produce radiation of short and bluer wavelength. The numbers of electrons contained in QDs depend on its size and structural shape, QDs can be having a single electron to a larger number of electrons. The adjustment of QDs size controls the number of electrons in a dot which greatly influence bandgap energy, therefore adjusting the size of QDs control the size of the bandgap. Since the emission frequency depends on bandgap size it's therefore possible to control the output wavelength with higher precision. This phenomenon makes the quantum dots to exhibit a novel property of broad absorption spectra and narrow size-tunable emission spectra [40].

2.3 Functionalization of QDs: Biocompatibility and Bio-conjugation

The CdSe and (CdSe) ZnS core/ shell QDs remain the most prominent, compatible and best available QDs for biological and biomedical applications [41, 42], such as diagnostics, biosensor and bio- labelling [43]. The high-quality QDs with longer photostability and high fluorescence quantum yield are synthesized with organic solvents. There are shortcomings regarding the application of QDs in biological media such as metallic toxicity, non-dissolubility and photo luminescence instability [44]. Based on these defects of QDs, it attracted a lot of research to improve the colloidal chemistry of QDs to increase biocompatibility and bio-stability to be applicable for bio system studies [45, 46].

QDs are often modelled through surface modification process, which involves the addition of a functional group to the QDs surface through ligand exchange process. The

ligands must have higher affinity to QDs surface and polar group for solubility in water [18]. The synthetics methods of QDs make use of polymers with outstanding biocompatibility and low toxicity to stabilize QDs nanocrystals in the fabrication of highly biocompatible polymer/QDs hybrid material [43]. Research has established five synthetic strategies of fabricating biocompatible polymer/QDs hybrid materials, which are ligand exchange; grafting polymer to QDs; grafting polymer from QDs; capping polymer on QDs and growing QDs within polymer template [47, 48]. Quantum dots such as CdSe, (CdSe) ZnS, CdTe and CdS/CdTe when synthesized with a large surface area they provide a larger binding site for many biomolecules of interest such as enzymes, antibodies, Herceptin and many biological proteins. In most of the bio-conjugation processes involves the aniline- catalyzed hydrazine bond formation and maleimide groups which are attached to the thiol functional groups [18].

Biocompatibility, solubility and surface coating of QDs for bio-conjugation are summarized in Figure 4.

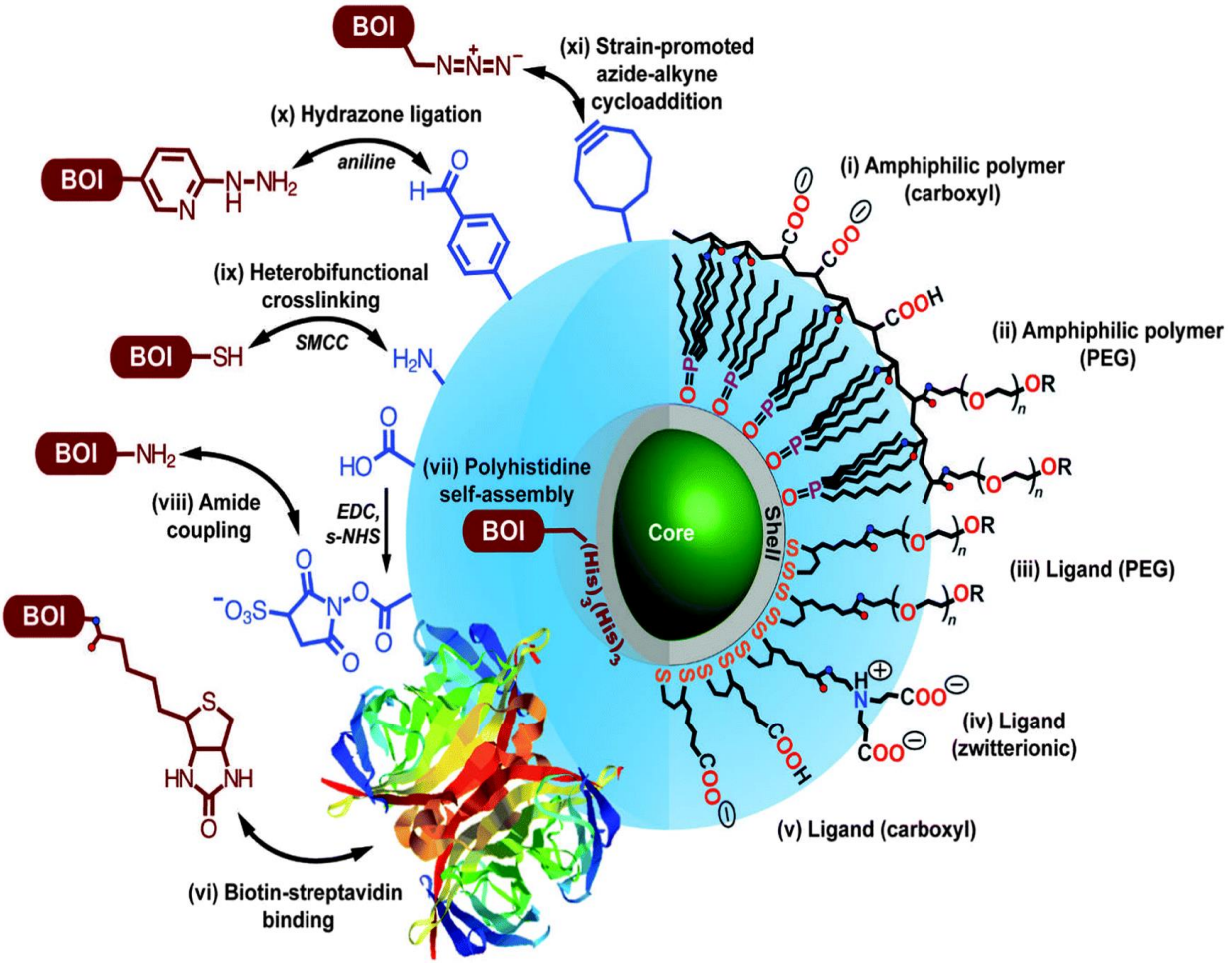

Figure 4: Summary of functionalization for core/shell QDs through ligand exchange on the right of the diagram: i-v and bio-conjugation on the left of the diagram: vi-x. BOI denotes any biomolecules of interest to be attached to the modulated surface of QDs. Adopted from [18].

2.4 Interaction of biocompatible QDs with biomolecules

Understanding the mechanism of interaction of QDs; CdSe, CdTe and (CdSe) ZnS with biomolecules; DNA, cells and proteins are of great significance in nanotechnology. It will lead to the development of bioengineered nanoparticles as light emitting devices, labelling agents and therapeutic proteins. The interactions of modulated QDs and biomolecules are studied using different instrumentation such as Fourier transform

infrared spectroscopy, atomic force microscopy, dynamic light scattering, circular dichroism spectroscopy, Raman spectroscopy, Fluorescence correlation spectroscopy and much other instrumentations [49, 50]. It's generally accepted that the interactions force that exists between the exogenous ligand of QDs and biological macromolecules include the physical electrostatic interaction, chemical bonding, hydrogen bonds, van der Waals interaction, hydrophobic force, host-guest chemistry, self-assembling of biomolecules on QDs surface and many more [51]. Several studies have established that physical electrostatic interaction is the most prominent interaction mechanisms in the bioconjugation system and hence it plays a vital role in stabilization of Protein-QDs complex [52]. The QDs surface modification depends on the properties and structure of the biomolecules to be conjugated with. The factors that affect the mechanism of interaction such as; binding constants, quenching constant and degree of cooperativity of NPs-Protein binding depend on the particle size and the protein structure.

2.4.1 Interaction of water-soluble CdTe Quantum dots with Bovine Serum Albumin (BSA)

The study conducted by Poderys et al [53], reported that the CdTe quantum dots coated with the thioglycolic acid (TGA) interacted with bovine serum albumin (BSA), the study employed different spectroscopic techniques such as dynamic light scattering, atomic force microscopy and electron spectroscopy. It was discovered that the addition of BSA protein to CdTe QDs increased the photoluminescence intensity of CdTe QDs and this change was detected up to BSA concentration of 10^{-5} $molL^{-1}$. The increase in BSA concentration in CdTe QDs solution have significantly decreased the photoluminescence.

The drastic change in photoluminescence intensity is due to the CdTe-BSA interaction. According to literature, the increase in photoluminescence intensity is caused by the decrease in non-radiative transitions [54]. The study demonstrates that the decrease in photoluminescence intensity is caused by the aggregation of CdTe QDs.

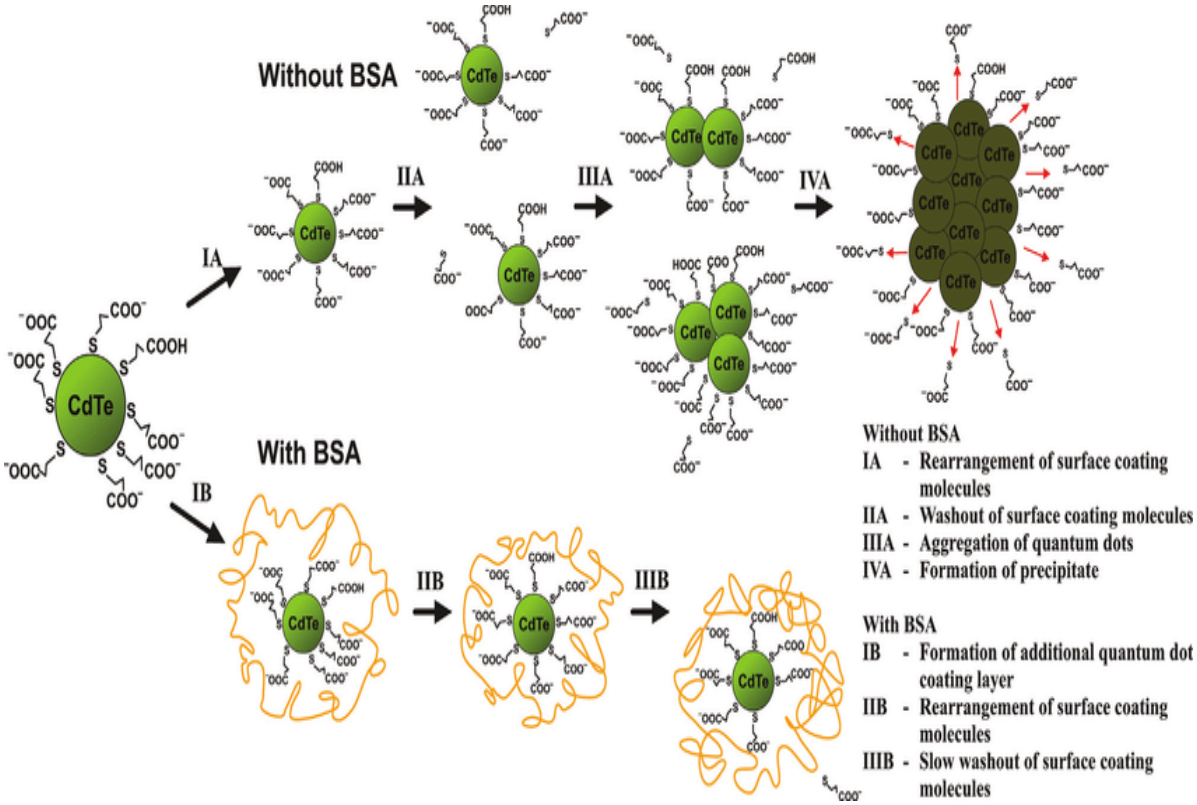

Figure 5: Schematic diagrams display the CdTe-TGA aggregation and the interaction of BSA with CdTe QDs. adopted from [53].

2.4.2 Interaction between CdSe quantum dots with haemoglobin

In accordance with the study by Hu *et al* [54] the interaction mechanisms of CdSe with haemoglobin (Hb) was examined using the spectroscopic methods. Theoretically, the UV-vis absorption spectroscopy has been applied to study the interaction that exists between the electron donor complexes and electrons accept complexes [55]. The study

conducted by Liu *et al* [56] reported that the CdSe is the electron transfer complex and Hb is an electron accept complex. Interestingly this study has confirmed the literature. The UV-vis absorption spectra showed a greater intensity at pH 6.0, which is being interpreted as the highest binding amount of CdSe QDs. It was discovered that the Hb increased the fluorescence of CdSe QDs at minimal concentration and quenches the fluorescence of CdSe at relatively higher concentration. The FTIR spectra revealed that there was no formation of a bond between CdSe QDs and Hb, hence the conclusion was drawn that the mechanisms of interaction between Hb and CdSe QDs is a result of electrostatic attraction and the surface-bound complexation equilibrium attraction that formed a stabilized CdSe-Hb complex.

2.4.3 Interaction of CdSe/ZnS core/shell quantum dots with maltose binding protein

According to a study by Kathiresan *et al* [57], the interaction of dihydrolipoic acid (DHLA) capped CdSe/ZnS with maltose binding protein (MBP) was studied using theoretical and computational chemistry. The comparison in optical properties of CdSe/ZnS core/shell and CdSe/ZnS- MBP complex were studied using quantum mechanics and ONIOM (QM/MM) (our own N-layered integrated molecular orbital + molecular Mechanics) calculations. In their QM/MM calculations, the QDs were treated with quantum mechanics and the entire system surrounding the QDs were considered molecular mechanically, hence the interface of QM/MM showed that the atoms were covalently bonded. The increase in absorption wavelength of QD-protein complex was observed which influenced the formation of ground state complex of DHLA capped CdSe/ZnS with binding site of MBP, the absorption energies of QD-protein is red shifted,

thus the protein stabilized the QDs and significantly enhance the absorption energies in comparison to the bare CdSe/ZnS core/shell. The calculation of light harvesting efficiency (LHE) was found to be higher for a bare CdSe/ZnS than the QDs-Protein complex; hence it gave an indication that the core/shell QDs is an ideal candidate for enhanced LHE. Similarly, the decrease in LHE value due conjugation of QDs-protein showed a strong interaction of CdSe/ZnS QDs with MBP protein.

2.4.4 Interaction between CdSe/ZnS core-shell quantum dots and bovine serum albumin (BSA)

The study by Dali *et al* [58], reported the interaction of CdSe/ZnS core/shell quantum dots with BSA protein using the fluorescence and UV-vis spectroscopy. They investigated the effect of temperature on the structural and spectroscopic properties of CdSe/ZnS QDs, BSA protein and the QDs-BSA conjugate. The incorporation of BSA to the surface of QDs resulted in the significant change in absorption spectra, as such a small blue shift was observed and a decrease in intensity of BSA characteristic band was detected. Those changes gave an indication of static interaction between the quantum dots and BSA protein, which resulted into the formation of QDs-BSA conjugate. Their fluorescence mechanisms enabled the determination of binding constant that exists between QDs and BSA protein which was found to be $1.05x10^7$, similarly, the number of the binding site per particle was calculated to be 2.32. Subsequently, it was discovered that there exists an electrostatic interaction between QDs and BSA protein, which resulted from the negatively charged QDs surface being attracted by the positive charge BSA protein. The effect of temperature was investigated by monitoring the change in

fluorescence emission of the tryptophan residue in both BSA protein and QDs solution through temperature variation in the range of 25˚C to 75˚C. It was discovered that increasing the temperature reduces the emission of QDs-BSA protein conjugate. This attribute demonstrates that after the bioconjugation, the QDs display a more complex temperature dependent fluorescence emission which is influenced by the thermal structural changes of the protein.

2.5 Application of Quantum Dots: Medical and Biological Studies

The most used quantum dots are CdS, CdSe/CdS, CdSe, ZnSe, CdSe/ZnS and CdTe, these colloidal semiconductors came to light as inform of a replacement of the traditional organic dyes and protein-based fluorophores which are used in biological, medicinal and natural sciences research works [59]. In comparison to the organic/protein fluorophores, QDs are stable and displays distinctive optical and electronic properties. They can withstand many cycles of excitation for a longer period of time [60], they have tuneable emission spectra which can be manipulated through the control of QDs particle size, in addition, the QDs have a higher photostability which is the most important tool for fluorescence imaging application [61]. In contrast, the organic dyes have relatively large emission spectra which often overlap with their fluorescence spectra which prohibit their application in multiplex imaging [62], they are also said to be not photo-stable and they have short-term aqueous stability.

The luminescent colloidal nanocrystals QDs have emerged as the most potent class of fluorescent probes for biomedical and cellular imaging which have been of greater

interest and applied in vitro and vivo studies. Prior to the unique fluorescent properties of QDs, the photo-luminescent nanocrystals QDs have been extensively studied in biomedical research of which its fundamental application is based on biosensing and imaging. Other biomedical applications include the drug delivery photodynamic therapy, diagnostic of foreign cells and diseases, tissue mapping and studying the intracellular process. The biological imaging applications of QDs involve the biofunctionalization of QDs that involves the coupling of QDs with biomolecules which trace and identify the specific receptors molecules to be labelled.

Table 1: Biomedical application of bio-functionalized QDs [36 -41].

	Bio-linkers	Biomolecules attached	Quantum dots	Application as biosensors
1	TOPO (trioctylphosphine oxide) along with MAA	Glycoproteins	CdSe	Label microorganisms, label specific cell type and lineages in vitro system
2	Primary-amine containing molecules using the activator EDC	Adenine and AMP	CdSe/ CdSe-ZnS	Labeling bacteria by Purine dependent mechanism
3	Alpha-fetoprotein antibody (AFP)	Tumour tissue	ZnS capped CdSe	Hepatic Cancer detection
4	Avidin	Antibody	CdSe-ZnS core	Detection of Cholera toxin
5	Tricosanthin (TCS)	Human choriocarcinoma cells (JAR cells)	ZnS capped CdSe	Treatment of AIDs
6	Streptavidin	DNA	Au-NPs	Detection of nucleic acids

2.6 Optical and electronic application of QDs

The most important optical and electronic properties of QDs are; the controllable large band gap structure, band mixing probabilities, spatial charge distribution and the ability to form multiple exciton generations (MEG) [34]. The band gap structure depends on the size of QDs, the smaller the QDs crystal the larger the band gap, which requires more energy for excitation and hence more energy is released during the relaxation process

[33]. The multiple generations of the electron/hole carrier in QDs is due to the intrinsic dipole moments of QDs nanoparticles which increase the charge separation/ distribution. The MEG has been reported in the nanoparticle material QDs such as PbSe, Si, CdSe, CdTe, InAs and CdSe/ZnS [34]. The above properties made the QDs to be potential candidates in optoelectronic devices such as photovoltaic, photodetector, photo electrochemical cells, Laser and light emitting diodes. In accordance to study by Jasim [72], demonstrated that the quantum dots solar cell devices use the MEG mechanism which provides high photo conversion efficiency and they are capable of harnessing large solar energy in the solar spectrum. In contrast to the traditional solar cells, the QDs solar cells have improved features such as lower power consumption, higher efficiency and increased electrical performance. Due to the optical properties of QDs, they can also be applied as Photodetector, for detecting both infrared and visible light [63]. The visible light photodetectors are used as image sensors which transform incident light into an electronic signal. QDs are very instrumental in the application of light emitting layers in LED devices, which are used for lighting; the backlighting and phosphors for white lighting or horticultural lighting.

2.7 *Moringa oleifera* seeds coagulant protein

Moringa oleifera tree belongs to the Moringacea family [1], a non-toxic tropical tree native of a Sub-Himalayan part of North West India, Pakistan, Afghanistan, Sub-Saharan Africa and Southern America [64, 65]. This tree is often referred to as a "miracle multipurpose" plant, because almost each of its component (roots, leaves, flower, seeds and bark) are beneficial to human health in the form of nutritional, medicinal and

therapeutic purpose [66]. Due to the invaluable quality of *M. oleifera* it gained lots of application in rural communities. It adapts in semi-arid climate hence is grown in many African countries for household purposes. Extensive studies were done on the application of *M. oleifera* seeds as natural coagulants in water treatment. Natural coagulants are regarded to be very efficient and safe for human consumptions, for this reason, native in developing countries has found their simple methods of treating water using the *M. oleifera* seeds. In accordance with the study by Eilert [67], it demonstrated the application of *M. oleifera* seeds in water treatment and it was discovered that the seeds contain a lower molecular cationic protein responsible for coagulation.

The coagulant protein extracted from *M. oleifera* seeds is characterized as a water-soluble dimeric cationic protein with a molecular weight of 6.5-13 kDa and an isoelectric pH in a range of 10-11 [68]. According to the study by Kwaambwa and Maikokela [69], they found that the protein conformation depends on the pH of the solution and its ionic strength is minimal at above pH 9. The molecular weights of this protein extract depend on the extraction process and the solvent of extraction used [70]. Kwaambwa and Maikokera [71] reported the secondary structural of *M. oleifera* seeds coagulant protein (MOCP) using the FTIR and CD spectroscopy, which was found have to have three amino groups amide I, amide II and amide III and the secondary structure was found to have more α-Helix content and smaller content of β-sheet. *M. oleifera* seeds protein has been applied as a coagulant in water treatment and purification process. The MOCP when added to raw water it generates a positive charge which acts as a magnet attracting and binding the negatively charged waste material and other toxic particle in water forming

flocs, which are then removed through settling or filtration [70, 72]. This process reduces hardness, turbidity, acidity, alkalinity and chlorine in water after treatment [33]. The coagulation mechanisms of MOCP have been explained in different ways. It can be described as a result of adsorption, charge neutralization and inter-particle bridging [73]. This proof of concept water treatment and purification gave hope and invited a lot of research studying the MOCP to find the permanent solution, cheap, human health friendly and large-scale water purification processes using saline water soluble MOCP. In addition to water purification, the study by Mangale *et al* [74], discovered that MOCP is antimicrobial active against micro-organisms present in water, specifically able to flocculate the Gram-positive and Gram-negative bacterial cell which reduces the number of bacteria in water.

The active coagulant protein extracted from *Moringa* seed has been studied extensively based on its adsorption ability and higher binding affinity, it has been used as biosorbent and has been applied as an adsorbent to remove pollutant and toxic compounds in water [75]. Hence it gained a lot of application in biosorption [72]. In addition, the MOCP has been applied for the removal of reactive dyes [76], organic pollutants and heavy metal from the aqueous solutions. The MOCP is used to remove humic acid in water [77].

2.7.2 Interaction of *M. oleifera* seeds protein with mineral surface and surfactants

Kwaambwa *et al* [78], suggested that the *M. oleifera* seed protein (MOP) has the ability to bind to a different material that has different polarity and isoelectric points. In their study they employed the neutron reflection technique to study the interaction of MOCP

with sapphire (α-Al_2O_3) both in the absence and in presence of a surfactant; Sodium dodecylsulfate (SDS) and Cetyltrimethylammonium bromide (CTAB). Their study demonstrated that the mechanism of interaction between the MOCP and α-Al_2O_3 was due to adsorption of MOCP to the sapphire interface. The neutron reflection measurements revealed the maximum amount of MOCP adsorbed to the surface of sapphire to be 5.3 ± 0.5 mgm^{-2}. The effect of water on the α-Al_2O_3-MOCP conjugate was investigated, and it was found that the protein did not desorb from the solid/liquid interface when rinsed with water. In their study they have also investigated the influence of surfactant on the adsorbed protein on sapphire (α-Al_2O_3-MOP); upon the addition of SDS, it has increased the reflectivity which indicated the co-adsorption. In addition, when the CTAB was added to the α-Al_2O_3-MOP matrix it significantly desorbed the protein from the interface. The conclusion was drawn from this study that the binding of MOCP is independent of the chemical nature of substrates, hydrophobic nature of the protein and hence can depend on other interaction mechanisms such as electrostatic interaction and adsorption.

2.7.3 Interaction of *M. oleifera* seeds coagulant protein with azo dyes and pesticide

The study conducted by Pavankumar and Sigh [79], reported the molecular interaction between *M. oleifera* coagulant protein and azo dyes (congo red, tartrazine) and a pesticide; dichlorodiphenyltrichloroethane (DDT). The study employed a computational simulation; the molecular docking tool Auto Dock 4.2 [76], which was used to compute the molecular interaction of the protein and ligands (pollutant). It was discovered that all these three ligands resulted into binding interaction with MOCP which formed plausible

stable MOCP ligand conformation. With respect to their calculated binding energy, Congo red was found to have the higher binding energy of -5.66 $kJmol^{-1}$, which could be associated with its large surface area and its polar functional groups. However, tartrazine binding affinity was found to be -5.33 $kJmol^{-1}$ and the least binding affinity was found to be -5.04 $kJmol^{-1}$ of DDT. In their study they have found that the strong binding affinity of MOCP with these ligands are results of the hydrogen bonding, electrostatic interaction and least minimum binding energy were contributed by the Van der Waal forces. As evident from this molecular interaction, it gave an indication that the MOCP has multiple binding sites which can form multiple interactions with other molecules. Due to the strong binding affinity of these pollutants with MOCP, these researchers have demonstrated an application of MOCP for removal of these dye and pesticide in water at laboratory level which was a proof concept. They have further suggested that the application of this multi-functional MOCP on water treatment may be applicable to large-scale and industrial water treatment.

2.7.4 Interaction of *M. oleifera* seeds coagulant Protein with anionic surfactants

The study by Maikokera and Kwaambwa [80], reported the use of viscometry, surface tension, fluorescence spectroscopy and circular dichroism spectral correlation coefficients to probe and study the mechanisms of interaction between the *M. oleifera* seeds coagulant protein (MOCP) and anionic surfactants sodium dodecyl sulfate (SDS) and sodium dodecyl benzene sulfonate (SDBS). By monitoring their intrinsic viscosity measurements, it was discovered that the addition of anionic surfactant to the protein has gradually increased the viscosity and then decreased upon the increased concentration

of surfactant at 0.768 mM. The further increase of surfactant concentration to 2 mM and above has resulted in the steady increase of the viscosity. According to these researchers, the change encountered in viscosity correlate to the literature that suggests a change in the conformation of the protein structure and aggregations [81] and the protein restructuring and expansion of protein molecule coil. The researcher showed that other mechanisms should have influenced the change in viscosity such as protein aggregation, surfactant binding and surfactant micellization. The plausible strong electrostatic interaction was said to be present at a low concentration of surfactant which stabilizes the protein-surfactant complexes. Several studies [78], done on the MOCP- surfactant system reported the cationic property of MOCP in water, which tend to attract anionic surfactant through electrostatic interaction to form a neutral charged MOCP-Surfactant complex. The interaction of MOCP with surfactant was found to be following the trending series of decreasing in strength interaction: anionic > cationic > zwitterionic / non-ionic [82-83].

CHAPTER 3: MATERIALS AND METHODS

3.1 Materials

All chemicals and solvents were purchased from Sigma-Aldrich or Merck and were used as received without further purification. Chemicals used were cadmium acetate dehydrate $(CH_3COO)_2Cd.2H_2O$), Highly pure selenium powder (Se), trioctyl-n-phosphene oxide (TOPO), trioctylphosphine (TOP), hexadecyl amine (HDA), tetradecyl-phosphonic acid (TDPA), sodium chloride (NaCl), petroleum ether, ammonium sulfate $(NH4)_2SO_4$, carboxymethylcellulose (CM-Cellulose microgranular 25-60 µm), toluene and methanol. *M. oleifera* seeds were purchased from a local supplier.

3.2 Synthesis of CdSe Quantum Dots

CdSe quantum dots were synthesized using the procedures outlined by Gupta *et al* [84], with minimal modification. In the typical recipe, 8.0102 g of TOPO was placed into a 250 mL three-neck flask. About 2.5048 g of HDA and 0.0520 g of TDPA were added to the reaction vessel (250 mL three-neck flask); the mixture was dried through heating at 100ºC for 30 minutes. TOPSe solution was prepared by dissolving 2.2011g of selenium powder into 10 mL of TOP with frequent stirring using magnetic stirrer for 5 minutes, then it was added to the reaction vessels and heated at 270ºC for 30 minutes. The cadmium stock solution was prepared by mixing 2.5180 g of cadmium acetate with 20 mL of TOP in a 50mL beaker with constant stirring for 5 minutes, and then it was added to the reaction vessels by means of injection during stirring. The mixture was then heated at 270ºC for 60 minutes. The reaction mixture resulted in nucleation of CdSe nanocrystals

as a red solution was obtained washed with methanol and centrifuged at 3000 rpm for 25 minutes three times. The sediment was heated in an oven at 70ºC for 48 hours.

3.3 Extraction and purification *of M. oleifera* seeds protein

Extraction and purification of *M. oleifera* seeds protein was conducted according to procedure by Kwaambwa *et al* [69-71] there were no deviations made. The seeds of *M. oleifera* were obtained from a local supplier. *M. oleifera* seeds were deshelled manually and ground into a fine powder using a blender. About 100 g of the seeds fine powder was dissolved into 500 mL of petroleum ether and stirred with a magnetic stirrer at 50ºC for 2 hours. The solution was then subjected to the suction filtration; the residual powder obtained was dried in air on a sheet of paper. About 80 g of the powder was dissolved into 200 mL of distilled water and stirred for 1 hour. The solution was then filtered using suction filtration to remove the bigger solid particles, the resultant filtrated was placed into a conical flask and placed into a fridge overnight and filtered by gravity filtration. Ammonium sulfate was added to the solution to saturation for the precipitation of the protein and stirred with the glass rod. The protein emerged out of solution in form of sticky paste due to the salting effect. The solution was then filtered using suction filtration and the solid residue was re-dissolved into 200 mL of distilled water. The content was transferred into a conical flask, kept in a fridge for overnight and filtered by gravity. The aqueous impure protein solution was filled into the boiled dialysis tubing and dialyzed against distilled water in 25 L container, water was changed twice a day for duration of 3 weeks. The protein solution was passed through a column containing the CMC paste. After loading the protein in CMC an equal volume of 1M NaCl was added to the column

for protein elution. The eluent was kept in the fridge overnight and then filtered by gravity. The protein solution was dialyzed against distilled water to remove the NaCl ions, and then finally freeze-dried. The purified *M. oleifera* coagulant seeds protein (MOCP) of molecular weight of 13kDa was obtained [69].

3.4 Synthesis QDs-Protein Complex: CdSe-MOCP$_n$

The aqueous CdSe-MOCP$_n$ complex was prepared by mixing the increasing concentration of MOCP (n = 10, 25, 50, 80, 100 mg/mL) with CdSe at a fixed concentration (5.23 x10^{-3} M) dispersed in toluene; the complexes were prepared in a buffer solution at pH 8 [12]. The mixtures were subjected to orbital shaker for agitation and homogenization at 25ºC for 25 minutes at speed of 150 rpm and yielded an aqueous CdSe-MOCP$_n$ Complex, where n denotes the different concentration of MOCP.

The solid CdSe-MOCP complex was prepared by dissolving the 50 mg of MOCP into 5ml of the CdSe of 5.23 x10^{-3} M in toluene solution, the mixture was homogenized with an orbital shaker at 150 rpm at 25ºC [12]. The resultant aqueous CdSe-MOCP (50 mg/mL) was placed on the round bottom flask and subjected to the Rotor evaporator at 120 rpm at a temperature of water bath of 40ºC. The semi-solid CdSe-MOCP was then subjected to freeze drier and the crystalline CdSe-MOCP nanoparticles were obtained.

3.5 Characterization techniques

The synthesized CdSe QDs and CdSe-MOCP complex nanoparticles were characterized for their crystal structure and phase using Bruker D2 XRD instrument with radiation angle in the range of 5 to 70˚ at 2θ, using Bruker Eva software. The surface morphology,

homogeneity and elemental composition of CdSe QDs and CdSe-MOCP were measured using transmission electron microscopy (TEM) and higher resolution transmission electron microscopy (HRTEM) using Tecnai 20 G^2 S-Twin TEM with *e*-beam voltage of 200 kV and JSM-IT300 Scanning Electron Microscopy (SEM). The physical adsorption of gas molecules and surface area of MOCP was studied using the Brunaver-Emmett-Teller (BET) technique using nitrogen gas (N_2) on Micromeritics Trista 3000 instrument.

3.6 Investigation of the interactions between CdSe QDs and MOCP

The mechanisms of interaction between CdSe QDs and MOCP were investigated by measuring the chemical and physical properties of the synthesized CdSe-$MOCP_n$. Functional groups was investigated using Fourier Transform Infrared Spectroscopy (FTIR), the spectra was recorded in the range of 4000-500 cm^{-1} using Opus software (version 6.5.6) on Bruker Platinum Tensor 27 ATR-IR Spectrophotometer. UV-Vis absorption and fluorescence emission spectra was recorded at 298 K temperature and at 313 K on the Perkin Elmer Lambda 35 and Perkin Elmer LS 45, respectively.

3.7 Data Analysis

3.7.1 The particle size of CdSe QDs and band gap of CdSe QDs and CdSe-$MOCP_n$

The particle size of CdSe QDs was measured by XRD using Debye Scherrer relation [85]:

$$D = \frac{0.91\,\lambda}{\beta Cos\theta} \quad (13)$$

Where D (nm) is the crystalline size, $\lambda(nm)$ is the X-ray wavelength, β is the line broadening and θ is the Bragg angle.

The particle size of CdSe QDs was estimated using UV-vis absorption spectra using the formula below [86]:

$D = (9.8127x10^{-7})\lambda^3 - (1.7147x10^{-3})\lambda^2 + (1.0064)\lambda$- 194.84…….. (14)

Where D (nm) is the particle size of given CdSe QDs of 5.23x10^{-3}M and $\lambda(nm)$ is the first exciton absorption peak of 546.5 nm.

The band gap of CdSe QDs and CdSe-MOCP$_n$ are calculated using the Tauc relation plot [87, 88].

Direct transitions: $(\alpha hv) = B(hv - E_g)^2$ … … … … … … … … … … … … … … … (15)

Indirect transitions: $(\alpha hv) = B(hv - E_g)^{\frac{1}{2}}$ … … … … … … … … … … … … … … … … (16)

Defining the parameter: α is the absorption coefficients, hv is the photon energy, B is a constant and E_g is the optical band gap. The transition energy (band gap) was obtained by the plot of $(\alpha hv)^2$ versus *hv* for direct transition and $(\alpha hv)^{1/2}$ versus *hv* for indirect transition. The direct band gap and indirect band gap were obtained by extrapolating the linear region to the energy X-axis where $(\alpha hv)^2 = 0$ and $(\alpha hv)^{1/2} = 0$, respectively [85].

3.7.2 Surface area and pore size of MOCP

The surface area and pore size of MOCP was analyzed using the BET- Surface area and the BET- Isotherm plot. From the surface area plot, a series of the equation is obtained:

$$\frac{P}{V_a(P_0 - P)} = \frac{1}{V_m C} + \frac{(C-1)}{V_m C}\left(\frac{P}{P_0}\right) \text{ … (17)}$$

$$\frac{1}{V_m C} = Intercept \text{ … (18)}$$

$$\frac{(C-1)}{V_m C} = Slope \ldots \ldots (19)$$

For the BET adsorption isotherm plot:

$$S_{BET} = \frac{4.355}{Slope + Intercept} \ldots \ldots (20)$$

$$C_{BET} = \frac{Slope}{Intercept} + 1 \ldots \ldots (21)$$

Where V_m is a monolayer volume, V_a is the adsorbed volume C = C_{BET} which is the BET constant and S_{BET} is the surface area.

3.7.3 The Stern-Volmer analysis

The binding constant and quenching constants of the CdSe-MOCP complex at different concentration of MOCP were calculated using the Stern-Volmer equation [89]:

$$\frac{F_0}{F} = 1 + K_{sv}[Q] \ldots \ldots (22)$$

$$K_{sv} = K_q \tau_0 \ldots \ldots (23)$$

F_0 is the fluorescence intensity of pure CdSe QDs and F is fluorescence intensities of protein (MOCP) in the absence and in presence of quencher (CdSe QDs), respectively. K_{sv} is the Stern-Volmer quenching constant and [Q] is the concentration of the quencher. K_q is the quenching constant and τ_0 is the lifetime of the excited state in absence of quencher. Equation (22) is equated to equation linear equation of straight line.

3.7.4 Scatchard relation

The number of binding sites (n) and the static quenching constant (K) which is the equilibrium constant in this present paper were calculated using the scatchard relation approximation. The thermodynamic parameter the Gibbs free energy ΔG^{θ}, the enthapy change ΔH^{θ}, and entropy change ΔS^{θ}, were calculated using the equations belows:

Scatchard relation:

$$log\left(\frac{F_0 - F}{F}\right) = LogK + nlog\,[Q] \quad \ldots\ldots(24)$$

$$\Delta G^{\theta} = -RT\,InK \quad \ldots\ldots(25)$$

$$In\left(\frac{K_2}{K_1}\right) = \left(\frac{1}{T_2} - \frac{1}{1}\right)\frac{\Delta H^{\theta}}{R} \quad \ldots\ldots(26)$$

$$InK^{\theta} = -\frac{\Delta H^{\theta}}{RT} + \frac{\Delta S^{\theta}}{R} \quad \ldots\ldots(27)$$

$$\Delta G^{\theta} = \Delta H^{\theta} - T\Delta S^{\theta} \quad \ldots\ldots(28)$$

where T is the temperature in (K) and R is the gas constant 8.314 $JK^{-1}mol^{-1}$. The interaction was carried temperature 298.15 K and 313.15 K. From the Scatchard relation plot [90], equation (24) was equated to equation of straight line, thus the slope is equal to n and y-intercept is logK. Therefore, the number of binding sites (n), and the binding constanst which is also reffered as equilibrium constanst (K) was obtained

CHAPTER 4: RESULTS AND DISCUSSION

4.1 The structural and morphological characterization of CdSe QDs.

The X-ray diffraction pattern provides information about the crystalline phase of the synthesized CdSe quantum dots and the average crystalline size in nanometer. Figure 6 shows the X-ray diffraction pattern of nano-crystalline CdSe QDs at 50ºC, it contains 3 broad peaks at a diffraction angle of 2θ = 26.55º, 43.87º and 51.93º in correspondence to the Miller indices or plane (101), (110) and (112), respectively. It was then found that the CdSe QDs have a hexagonal (wurtzite) phase [84].

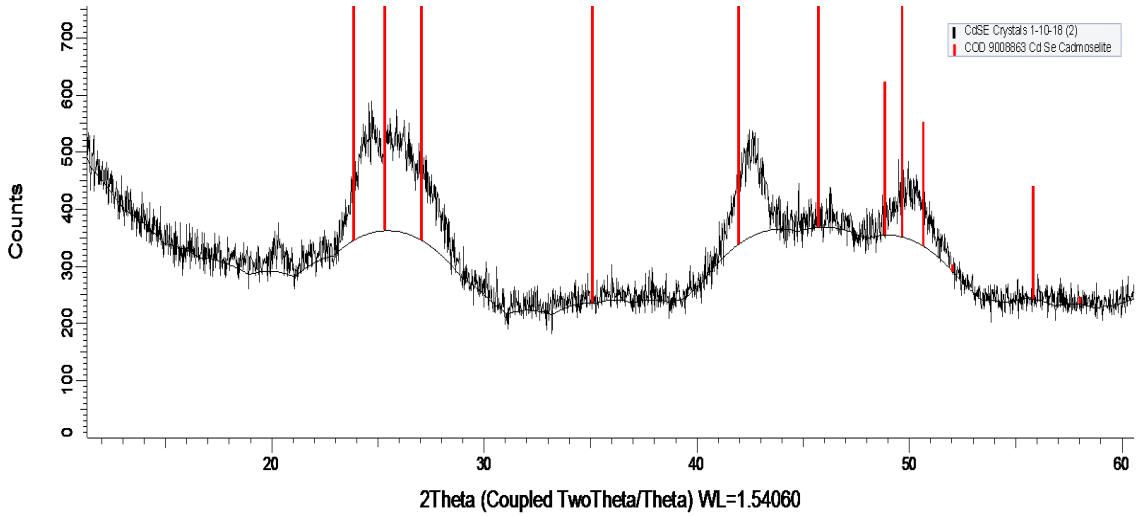

Figure 6: Powder X-ray diffraction pattern of CdSe QDs.

The crystallite sizes of CdSe QDs were estimated using the XRD between which was 3.1 to 8.1 nm. The variation in the particle size can be a result of the strain field [85]. The surface morphology of CdSe QDs was studied using HRTEM; the TEM image shows an even distribution to nearly spherical crystalline particles of CdSe QDs at 10 nm (Figure 7). The particles size using TEM was estimated to be in the range of 3.5 to 7.1 nm, which

is similar to the XRD crystals size of QDs. The surface morphology of CdSe-MOCP was investigated using the SEM at the scale of 1mm as shown by Figure 8; the image shows the larger particle of CdSe-MOCP complex. It was then observed that there is no uniform distribution of particles of CdSe-MOCP, hence, it is not a crystalline structure. Figure 9 shows the EDX micrograph of CdSe QDs which reveal the elemental composition present in CdSe QDs the ration in percentage by weight (%) of Cd: Se was found to be 1:0.8. It also showed the presence of other elements such as carbon, oxygen, phosphorus and chlorine, which may have resulted from the organic solvents, used such trioctyl-n-phosphene oxide, trioctylphosphine and other chemical reagents used during the synthesis of CdSe QDs. The elemental composition is summarized in Table 2.

Table 2: Bulk elemental composition of CdSe QDs

Element	**Cd**	**Se**	**C**	**O**	**Cl**	**P**
Wt. (%)	26.64	20.90	38.50	8.43	0.72	4.81

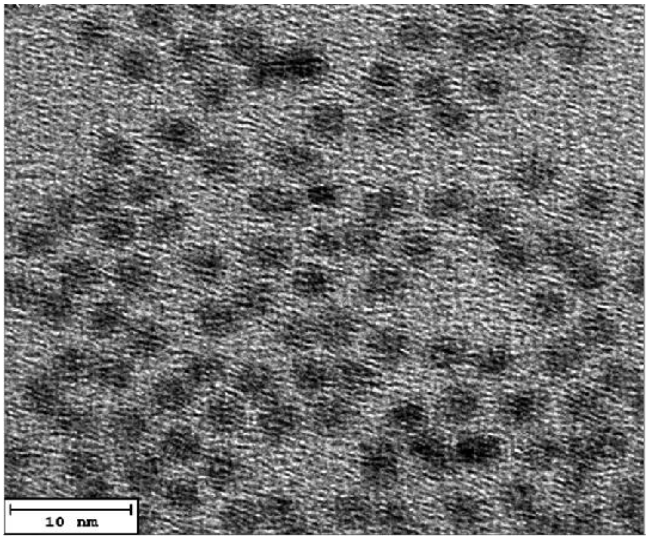

Figure 7: CdSe QDs: Nanocrystals (HRTEM image).

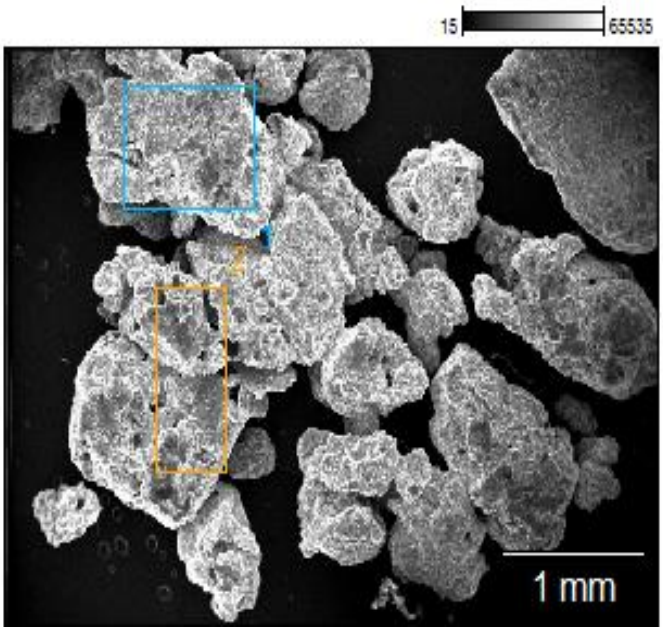

Figure 8: CdSe-MOCP Complex (SEM image).

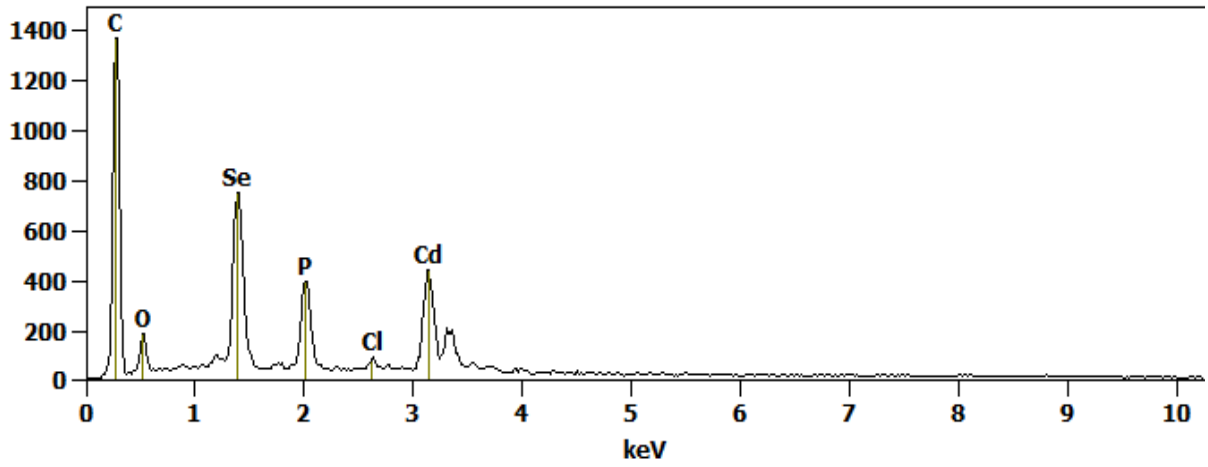

Figure 9: EDX micrograph of CdSe QDs.

4.2 Physical adsorption and pore size analysis of *Moringa* oleifera coagulant seeds protein

The BET theory was used to determine the surface area of MOCP and its pore size was determined using the BET isotherm plot. Figures 10 and 11 show adsorption of N_2 gas on

MOCP. BET isotherm, gives accurate account of adsorption isotherm only within restricted pressure range, i.e. $0.05 \leq P/Po \leq 0.35$.

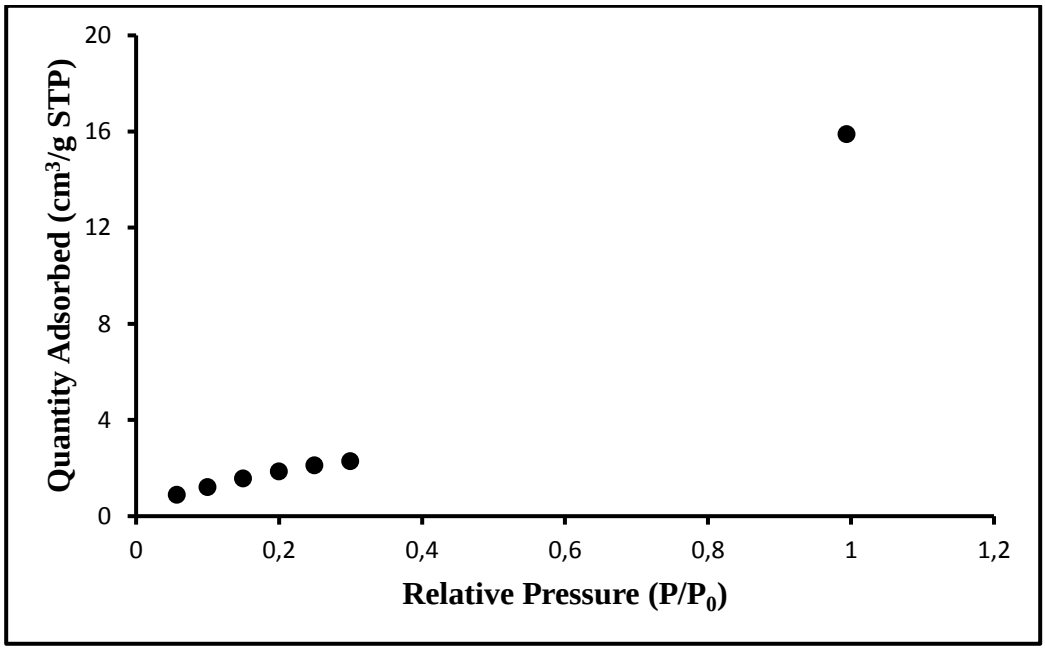

Figure 10: Adsorption isotherm of N_2 gas on MOCP.

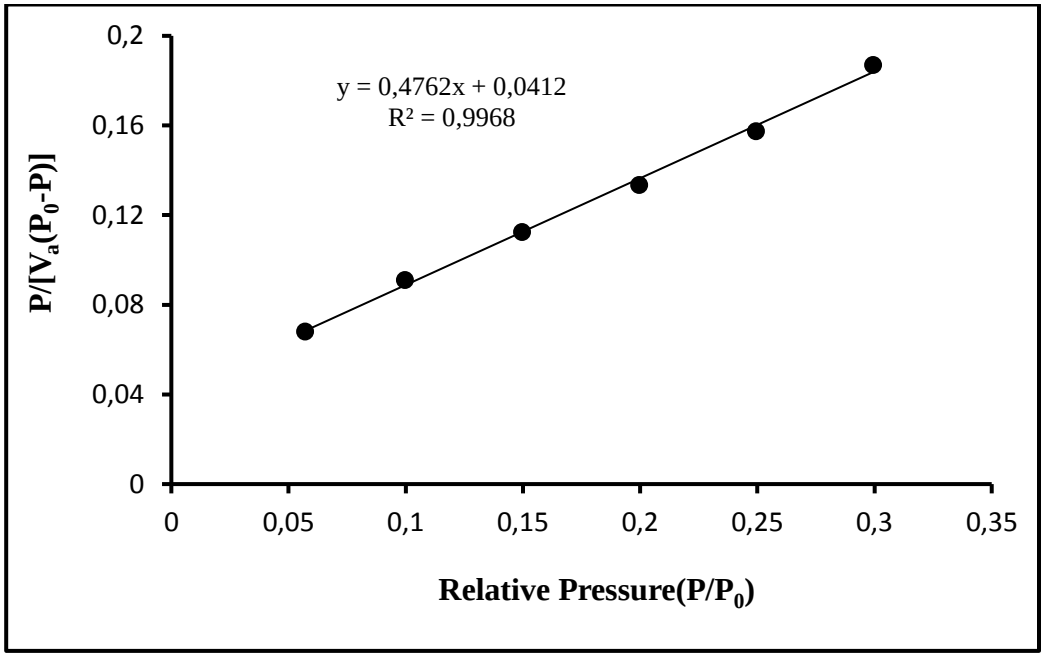

Figure 11: BET linear plot of the adsorption isotherm of N_2 gas on MOCP.

The BET surface area of MOCP was calculated to be 8.41 m^2/g. The pore volume at single point adsorption total pore volume of pores less than 302 nm diameter at P/P_0 = 0.9936 was 0.0245 cm^3/g. The pore size of MOCP was calculated to be 11.7 nm, thus the *M. oleifera* seed coagulant protein is classified as mesoporous [91]. The mesoporous pores of MOCP can be applied to host many guest molecules such as fluorescent imaging agents, such as CdSe quantum dots and other molecules can adsorbed into MOCP mesopores. Hence, the MOCP have a higher adsorption capability toward other molecules such as surfactant and charged particle [91, 92].

4.3 Interaction between CdSe QDs and MOCP using the UV-Vis absorption spectra

The interaction between CdSe QDs and MOCP in aqueous solution was characterized using the UV-Vis absorption spectroscopy.

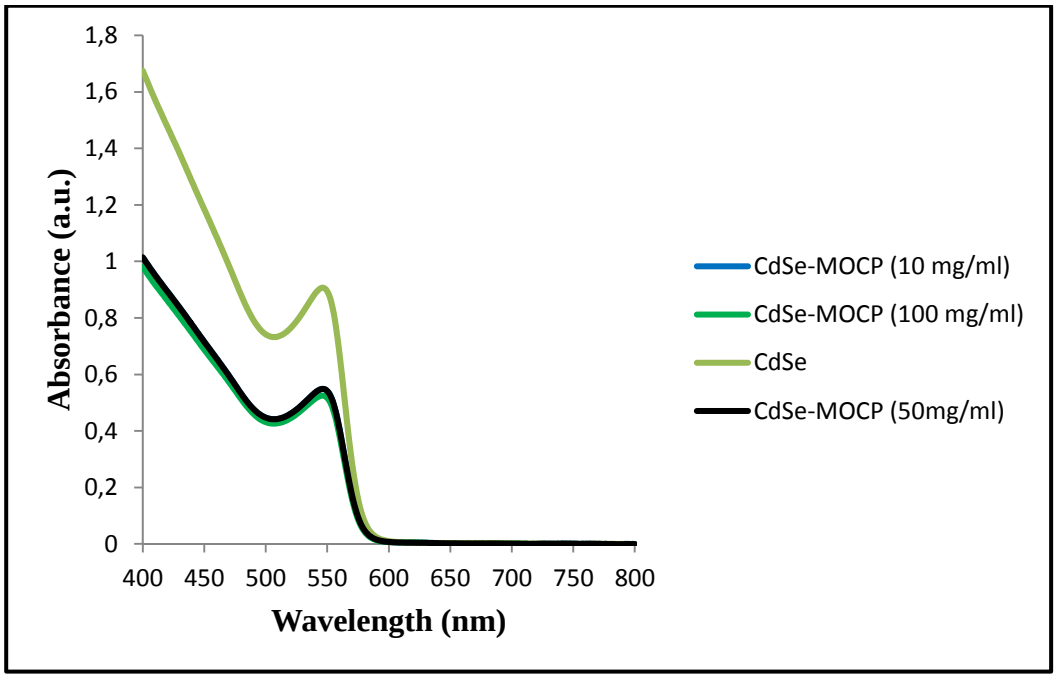

Figure 12: The UV-vis absorption spectra of pure CdSe QDs and CdSe-MOCP with the concentration of MOCP (10, 50 and 100 mg/mL).

As shown in Figure 12, the absorption peak at 546.5 nm is characterized as the absorption band of CdSe QDs. There was no new band observed upon the incorporating of CdSe QDs into MOCP. Upon the mixing of CdSe solution (5.23×10^{-3} M) with the different concentration of MOCP (10, 50 and 100 mg/mL) a sudden decrease in absorption intensities with a minimal sensitive shift in absorption band was observed accompanied by a blue shift of 3.5 nm of the maximum absorption band of CdSe QDs. The change in the absorption spectra indicates the presence of strong interaction between CdSe QDs and

MOCP which can be attributed to molecular complexation in formation of the CdSe-MOCP stable conjugates. The resultant change in absorption intensity may indicate that the tryptophan residues in the MOCP were in the hydrophobic environment [93, 94]. The particle size of CdSe QDs was estimated using UV-Vis absorption spectra and was found to be 3.1 nm [86].

4.3.1 Effect of MOCP on the band gap structure of CdSe QDs

The band gap structure of CdSe QDs and CdSe-MOCP at different concentrations of MOCP was studied using the Tauc plot, to determine the energy of direct and indirect band gap. As shown in Table 3, it was found that the direct band gap of CdSe QDs is 2.17 eV and the indirect band gap of 2.10 eV, both values are greater than the literature band gap of CdSe QDs which is 1.74 eV [84]. The band gap increased with an increase in concentration of MOCP of the CdSe-MOCP complex, this demonstrates that the incorporation of MOCP into CdSe QDs reduces the photo-activity of CdSe QDs by covering the active sites of CdSe QDs [95].

Table 3: Direct and indirect band gap of CdSe QDs and CdSe-MOCP complex

	Direct bang gap (eV)	**Indirect band gap (eV)**
CdSe QDs	2.17	2.10
CdSe-MOCP (10 mg/L)	2.19	2.12
CdSe-MOCP (50 mg/L	2.20	0.85
CdSe-MOCP (100 mg/L)	2.21	0.87

4.4 Interactions between CdSe QDs and MOCP using fluorescence spectra

The fluorescence emission spectra was used to study the interaction between CdSe QDs and MOCP in aqueous solution at a temperature of 298.15 K. The fluorescence (FL) spectroscopy revealed the excitation wavelength of MOCP and CdSe QDS at 302.7 nm and 602.4 nm.

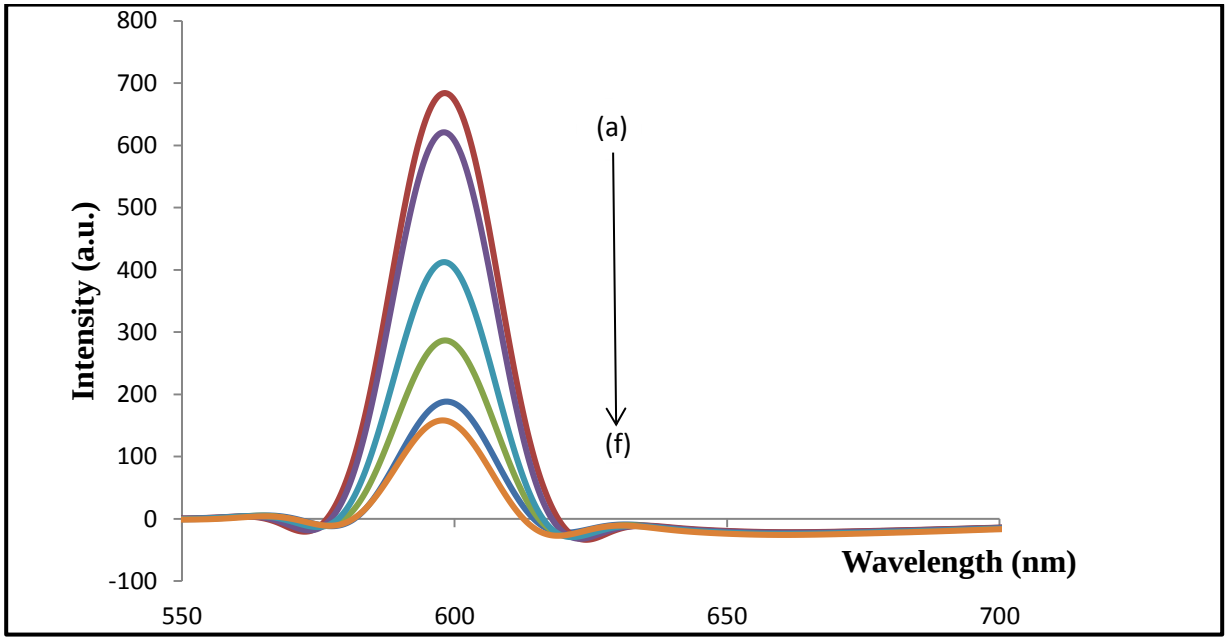

Figure 13: Fluorescence spectra of CdSe QDs as function of MOCP concentration in mg/mL; (a) 0, (b) 10, (c) 25, (d) 50, (e) 80, (f) 100. The concentration of CdSe QDs = 5.23 x 10^{-3}M and excitation wavelength = 602.4 nm.

FL spectra shown in Figure 13 was obtained by increasing the concentration of MOCP (10, 25, 50, 80,100 mg/mL) to a fixed concentration of CdSe solution (5.23 x 10^{-3} M) and the fluorescence intensities were measured. On the fluorescence spectrum, a reduction in fluorescence intensity was observed with increasing concentration of MOCP. The fluorescence intensity of CdSe QDs in absence of MOCP, which is denoted as F_0 is 683.7 nm. At a very low concentration of 10mg/mL, there was a minimal decrease in

fluorescence intensity. However, sudden decreases in the fluorescence intensities were observed at a higher concentration of MOCP. Thus fluorescence quenching is higher at high concentration of MOCP. The quenching of fluorescence emission results from the dynamic or static interaction between a quencher and fluorophore [96]. In many interaction studies of quantum dots and protein, QDs have quenched the protein [53-59]. However in the present study the FL spectra showed a strong quenching effect of MOCP in the fluorescence of CdSe QDs which is higher at higher concentrations of MOCP. The MOCP emit strong intrinsic fluorescence due to the presence of tryptophan residues, which are the amine constituents of the MOCP. According to the study by Yan *et al* [97], the combination of protein with QDs interaction changes the external environmental and structure of protein, which yield a decrease in fluorescence intensity. Hence, a similar explanation can be applied in the quenching between MOCP and CdSe QDs. There exist a strong interaction between CdSe QDs and MOCP as reflected by the steady decrease in fluorescence that give rise to the quenching mechanisms [93]. The quenching effect may results from many molecular interaction mechanisms, such as surface-bound complexation equilibrium, energy transfer, ground state complex formation [96, 98], molecular rearrangement [54], the electrostatic interaction [52] and the energy transfer process between the CdSe QDs and MOCP [99].

The quenching mechanisms between MOCP and CdSe QDs was found to be static quenching which is confirmed by the changes observed in the absorption spectra of the UV-Vis absorption analysis. [96]. Dynamic quenching is caused by the collision and energy transfer from the protein to the quencher; implying that there would be no

observable change in the MOCP UV-Vis absorption spectrum [93, 96-99]. To study the static quenching mechanisms, the estimation of binding constants (K_b) and quenching constants (K_q) is analyzed using the Stern-Volmer plot [89]. Stern-Volmer plots establish the linear relationship between the relative fluorescence of the CdSe-$MOCP_n$ intensity and concentration of quencher (MOCP).

4.5 Stern-Volmer Analysis of the CdSe QDs –MOCP interactions

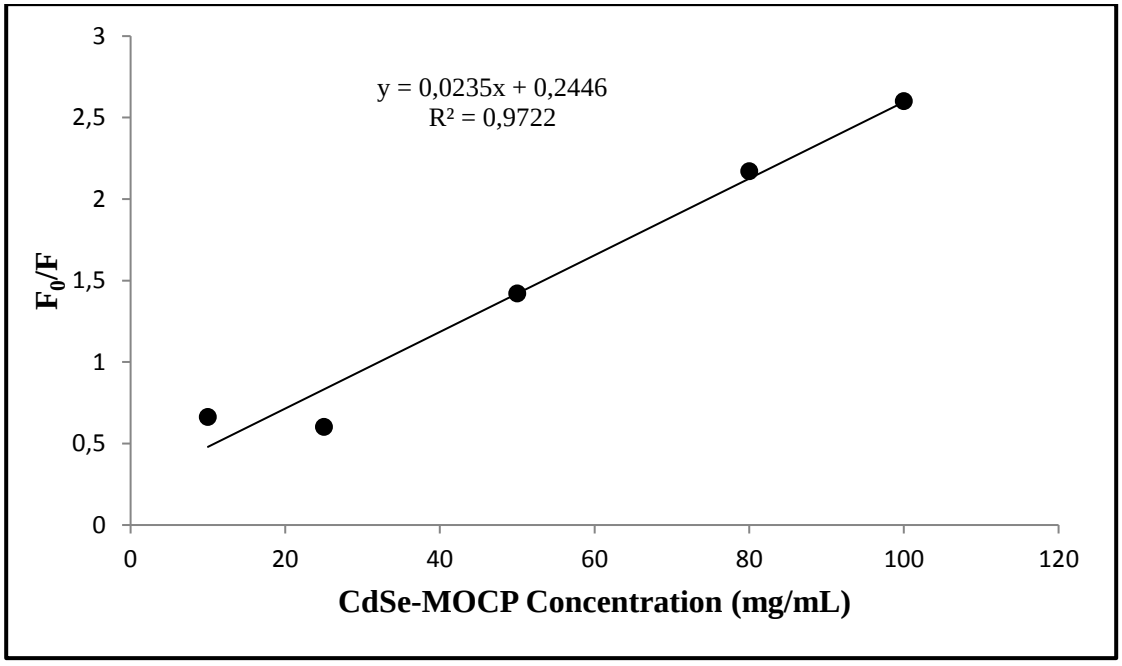

Figure 14: Stern-Volmer equation analysis of the CdSe-MOCP system: the figure shows the plot of the ratio for relative fluorescence (F_0/F) versus increasing concentration of MOCP in mg/mL.

Based on the Stern-Volmer plot: at a very low concentration of the MOCP (10 and 25 mg/mL), there was no significant change in the quenching effect, which suggests that there is minimal quenching to nearly stationed fluorescence quenching [12]. A steady increase in the quenching effect was observed upon the increase in concentration of

MOCP (50 mg/mL to 100 mg/mL) which suggest a strong interaction and conformational change in the MOCP structure and hence it indicates the possible existence of more binding sites and a higher affinity of MOCP toward the CdSe QDs [100]. From the linear plot the Stern-Volmer quenching constants (Ksv) was obtained as 0.0235. However the different parameters such as binding constant (K_b) and the quenching constant (Kq) at different concentrations of CdSe-MOCP complex were calculated using equation 13. The lifetime $\tau_0 = 1.91 \times 10^{-9}\ s^{-1}$ of the excited state of CdSe QDs in absence of MOCP [58].

Table 4: Stern-Volmer equation and analysis derived from the Stern-Volmer plot [49].

Stern-Volmer constant (K_{sv})	**Binding constant K_b (a x10^7 mL/mg)**	**Quenching constant K_q (b x10^7 mL/mgs)**
0.0235	0.0178	1.97

4.6 Thermodynamic parameters and binding mode of static quenching mechanism

The static quenching mechanisms of MOCP with CdSe QDs were analysed using the modified Stern-Volmer equation known as Scatchard method [90].

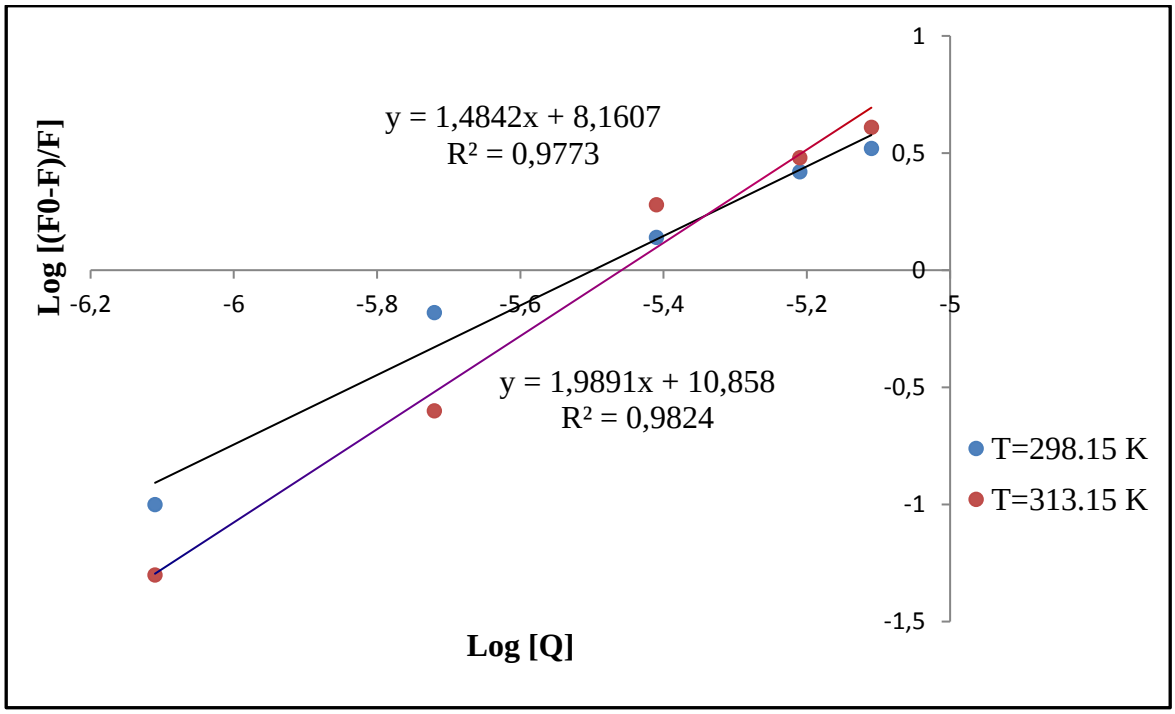

Figure 15: Scatchard relation represented by the plot of log [(F_0-F)/F) versus log [Q] at temperatures 298.1 K and 313.15 K respectively.

The number of binding sites was found to be 1.50 and 2.00 for temperatures 298.15 K and 313.15 K. The static quenching constant was determined as K= 1.45 x 10^8 and 7.21 x 10^{10} at temperature (T) 298.15 K and 313.15 K, respectively. The enthalpy change (ΔH^{θ}) was calculated to be -321.3 kJmol^{-1}, a negative value and ΔS^{θ} was found to be 156.0 JK^{-1}mol^{-1} a positive value, based on these values it gives an indication that the binding mechanisms of MOCP with CdSe QDs is entropically driven [101, 102].

The change in Gibbs free energy (ΔG^{θ}) was calculate to be -46.6 kJmol^{-1} at 298.15 K and -65.1 kJmol^{-1} at 313.15 K; negative value indicates that the binding interaction is spontenous [103]. The negative values of both ΔH^{θ} and ΔG^{θ} reveals that that the major interaction mechanisms is the electrostatic interaction, van der Waals forces and hydrophobic interaction [100-103].

Table 5: Calculated thermodynamic potentials and the number of binding sites.

Temperature (K)	**Number of Binding sites (n)**	**Equilibrium constant (K)**	**ΔG^{θ} (kJmol^{-1})**	**ΔH^{θ} (kJmol^{-1})**	**ΔS^{θ} (JK^{-1}mol^{-1})**
298.15	1.50	1.45 x10^{8}	-46.6	-321.3	156.0
313.15	2.00	7.21 x 10^{10}	-65.1		

4.7 FTIR Spectra Analysis

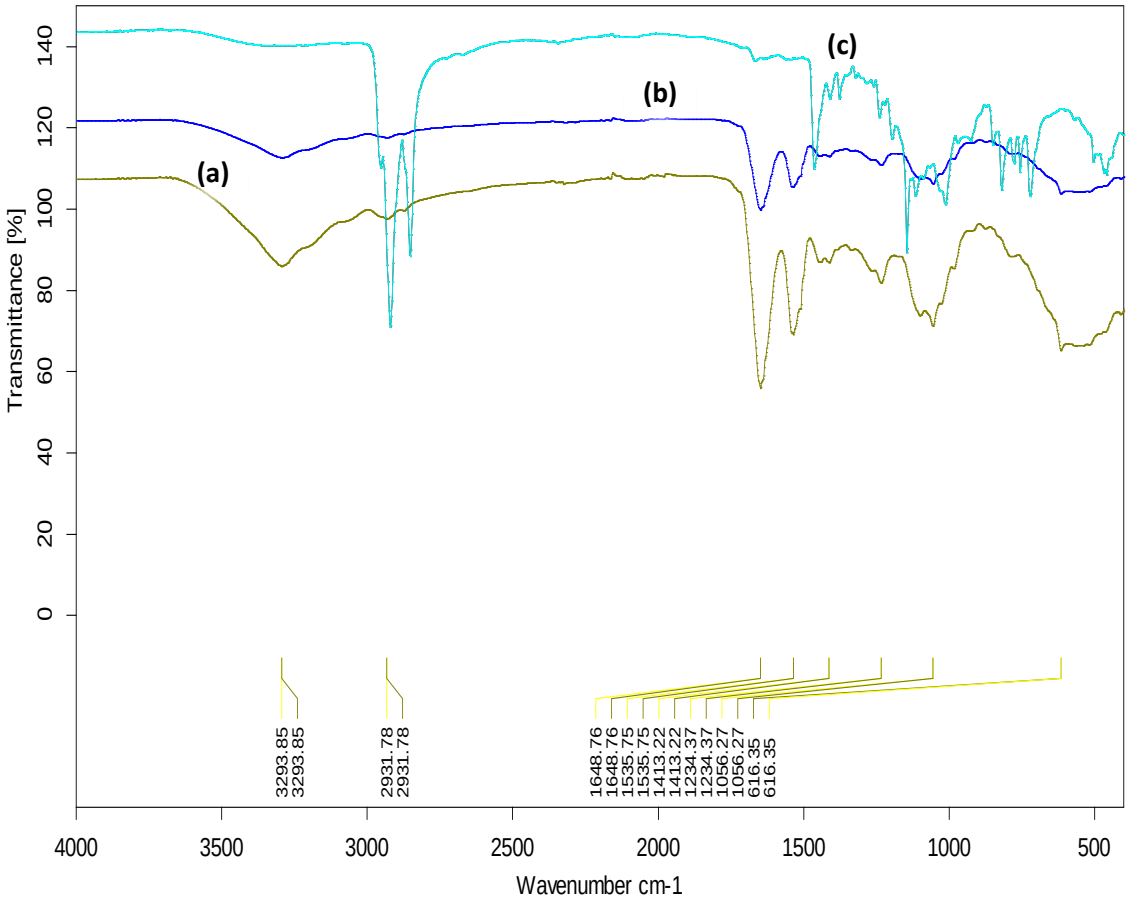

Figure 16: Diagram represents the FTIR spectra of CdSe QDs and MOCP. (a) MOCP; (b) CdSe-MOCP; (c) CdSe QDs.

The functional groups of CdSe QDs, CdSe-MOCP and MOCP, were investigated using FTIR spectroscopy in the spectrum range of 4000-500 cm^{-1}. Figure 14(a) shows the spectrum of *M. oleifera* coagulant seeds protein, notable absorption peaks of phenol group at 3293.85 cm^{-1}, primary amine at 1648.76 cm^{-1}, 1535.75 cm^{-1} nitro group and an Aliphatic amine at 1234 cm^{-1}. The functional group of the two absorption bands at 1648.76 cm^{-1} and 1535.75 cm^{-1}, shows the presence of the amide I and amide II functional group [6, 104-105]. The band at 1535.75 cm^{-1} can also indicate the presence of the α-

helices [104]. In comparison, Kwaambwa and Maikokera [6] showed presence of α-helix secondary structure given by band at 1291 cm^{-1}, which is absent in FTIR spectrum of MOCP, thus this shows the difference in structure of MOCP depending on method of extraction and purification used [4]. In Fig. 14(b) shows the spectrum of CdSe-MOCP at a concentration of 50 mg/mL of protein. The spectrum is identical to the one of MOCP, hence a conclusion can be drawn that there is new functional group and binding mechanisms between the CdSe QDs and MOCP [54]. The formation of the new bond could have changed the CdSe-MOCP spectrum thus the CdSe QDs did not influence the chemical structure of MOCP. There is a possibility that CdSe QDs are adsorbed into the MOCP by means of electrostatic interaction and surface-bound complexation equilibrium attractions which correlate to the fluorescence quenching mechanisms and the UV-Vis absorption spectra [94].

Tables 6 and 7 summarize the IR analysis of CdSe QDs and MOCP, which displays the bond and functional groups present.

Table 6: IR analysis of CdSe QD

No	**Wave number**	**Chemical Bonding**	**Functional group**
1	2931.78	C-H	Alkane
2	1413.22	C-H, C=C	Methyl group, aromatic
3	1234.37	C-O, C-X, or C-N	Ester, alkyl halide, aliphatic amine
4	1056.27	C-O	Primary alcohol
5	616.36	C	Elemental carbon

Table 7: IR analysis of *M. oleifera* coagulant seeds protein

No	**Wave number**	**Chemical Bonding**	**Functional group**
1	3293.85	O-H	Alcohol or phenol
2	2931.78	C-H	Alkane
3	1648.76	N-H	Primary amine; Amide I
4	1535.75	C=C or N-O	Aromatic or nitro group
5	1234	C-N	Aliphatic amine; Amide II
6	616.35	C-Cl	Alkyl halide

CHAPTER 5: CONCLUSION AND RECOMMENDATIONS

5.1 Conclusion

The CdSe QDs were synthesized using organic solvents trioctyl-n-phosphene oxide (TOPO) and trioctylphosphine (TOP). The crystalline size of CdSe QDs was determined by UV-Vis absorption to be 3.1 nm. XRD analysis revealed that CdSe QDs has a hexagonal phase with a particles size of 3.1-8.1 nm. The HRTEM image showed an even distribution, spherical surface of CdSe QDs and confirmed the crystalline size CdSe QDs at 10 nm scale. The EDX micrographs of CdSe QDs revealed the ratio Cd: Se to be 1:0.8 and showed the presence of other elements present in the CdSe QDs matrix. The BET analysis determined the surface area and pore size of MOCP and it was classified as mesoporous. The SEM image indicated that CdSe-MOCP complex is not a crystalline structure. The interaction of CdSe QDs with increase in concentration of MOCP showed a decrease in fluorescence intensity which is classified as static quenching, UV-vis absorption spectra revealed the possibility of complexation between CdSe and MOCP, which was confirmed by the calculated values of Stern-Volmer quenching constant (K_{sv}), binding constant (K_b), quenching constant (K_q) and the number of binding sites (n).. The thermodynamic potentials were calculated using the Scatchard equation, $\Delta G^{\theta} < 0$, $\Delta H^{\theta} < 0$ and $\Delta S^{\theta} > 0$ which indicates that the binding mechanisms is entropic favoured and spontaneous; it also demonstrated that the stable CdSe-MOCP complex is a result of electrostatic interaction, molecular complexation and presence of hydrophobic interaction and Van der Waals forces.

5.2 Recommendations

The study on the interaction of *M. oleifera* seeds coagulant protein and CdSe QDs discovered that a stable CdSe-MOCP complex was formed by electrostatic interaction, molecular complexation and hydrophobic and Van der Waals forces. The study was aimed at exploring the physicochemical properties of MOCP such as charge characteristics, structure conformational change of CdSe-MOCP and hence the specific active component in MOCP responsible for interaction with CdSe QDs, however the objective was not attained due to the lack of expensive instrumentation required such as Photoluminescence Spectroscopy, Raman Spectroscopy and Circular dichroism measurements. Hence a further well-funded research is needed to fill the gap. On the present results, CdSe-MOCP was found to be stable with increasing concentration of MOCP as revealed by the quenching constants, this information will help in research areas such as studying CdSe-MOCP as fluorescent probes, sensors, labeling agent and application of CdSe-MOCP in water treatment.

CHAPTER 6: REFERENCES

[1] Muyibi SA, Evison LM. Optimizing physical parameters affecting coagulation of turbid water with *Moringa oleifera* seeds. *Water Research.* 1995; 29(12): 2689-2695. Available from: https://doi.org/10.1016/0043-1354(95)00133-6.

[2] Muyibi SA, Evison LM. Optimizing physical parameters affecting coagulation of turbid water with *Moringa oleifera* seeds. *Water Research*. 1995; 29(12): 2689-2695.

[3] Ndabigengesere A, Narasiah KS, Talbot BG. Improvement of the flocculation process in water treatment by using *Moringa oleifera* seeds extract. *Water Research*. 1995; 29: 703-704.

[4] Kwaambwa HM, Maikokera R. A fluorescence spectroscopic study of a coagulating protein extracted from *Moringa oleifera* seeds. 2007; 60(2): 213-220. Available from: https://doi.org/10.1016/j.colsurfb.2007.06.015.

[5] Martyn CN, Osmund C, Edwardson JA, Barker DJP, Harris EC, Lacey RF. The geographical relation between Alzheimer's disease and aluminium in drinking water. *The Lancet*. 1989; 333(8629):59-62. Available from: https://doi.org/10.1016/S0140-6736(89)91425-6.

[6] Kwaambwa HM, Maikokera R. Infrared and circular dichroism spectroscopic characterization of secondary structural components of a water treatment coagulant protein extracted from *Moringa Oleifera* seeds. *Colloids Surfaces B: Biointerfaces*. 2008; 64(1): 118-125.

[7] Mathew S, Bhardwaj BS, Saran AD, Radhakrishnan P, Nampoori VPN. Bellare JR. Effect of ZnS shell on optical properties of CdSe/ZnS core-shell quantum dots.

Optical materials. 2015; 39: 46-51. Available from: https://dx.doi.org/10.1016/j.optmat.2014.10.061.

[8] Joglekar SS, Gholap HM, Alegaonker PS, Kale AA. The interactions between CdTe quantum dots and protein: Understanding nano-bio interface. *Journal of Material Science*. 2017; 4(1): 209-222. Doi: 10.3934/matersci.2017.1.209.

[9] Kim J, Lee J, Kyhm K. Surface Plasmon assisted modal gain enhancement in Au-hybrid CdSe/ZnS nanocrystal quantum dots. *Applied Physics letters*. 2011; 99(21): 213112. Available from: https://doi.org/10.1063/1.3664114.

[10] Mattoussi H, Mauro JM, Goldman ER, Anderson GP, Sundar VC, Mikulec FV, Bawendi MG. Self-assembly of CdSe-ZnS quantum dots bioconjugates using an engineered recombinant protein. *Journal of the American Chemical Society*. 2000; 122(49): 12142-12150. Doi: 10.1021/ja002535y.

[11] Wang JH, Liu TC, Cao YC, Hua XF, Wang HQ, Zhang HL, Li XQ, Zhao YD. Fluorescence resonance energy transfer between FITC and water-soluble CdSe/ZnS quantum dots. *Physicochemical and Engineering Aspects*. 2007; 302(1-3):168-173. Available from: https://doi-org-ezproxy.unam.edu.na/10.1016/j.colsurfa.2007.02.018.

[12] Liang J, Cheng Y, Han H. Study on the interaction between bovine serum albumin and CdTe quantum dots with spectroscopic techniques. *Journal of Molecular Structure*. 2008; 892(1-3); 116-120. Available from: https://doi-org.ezproxy.unam.edu.na/10.106/j.molstruc.2008.05.005.

[13] Kastner M. Physics today: artificial atoms. *Journal of American Institute of Physics.* 1993: 24-27.

[14] Galian RE, Guardia M. The use of quantum dots in Organic Chemistry. *Trends in Analytical Chemistry*. 2009; 28(3): 279-291. Doi: 10.1016/j.trac.2008.12.001.

[15] Mishra S, Panda B, Rout SS. An elaboration of quantum dots and its applications. International Journal of Advances in Engineering and Technology. 2012. ISSN 2231-1963.

[16] Alivisatos AP. Perspectives on the physical chemistry of semiconductor nanocrystals. *Journal of Physical Chemistry*. 1996; 100: 13226-13239.

[17] Bruchez JM, Maronne M, Gin P et al. Semiconductor nanocrystals as fluorescent biological label. *Journal of Science*. 1998; 281: 2013-2016.

[18] Chan WC, Nie S. Quantum dots bioconjugates for ultra-sensitive nano-isotopic detection. *Journal of Science.* 1998; 281: 2016-2018.

[19] Wu X, Liu H, Liu J et al. Immunofluorescent labeling of cancer marker Her2 and other cellular targets with semiconductor quantum dots. *Journal of National Biotechnology*. 2003; 21: 41-46.

[20] Han M, Gao X, Su JZ et al. Quantum-dot-tagged microbeads for multiplexed optical coding of biomolecules. *Journal of National Biotechnology*. 2001; 19: 631-635.

[21] Medintz IL, Uyeda HT, Goldman ER et al. Quantum dot bioconjugates for imaging, labelling and sensing. *Journal of Natural Material Sciences.* 2005; 4: 435-446.

[22] Sahoo SK, Labhasetwar V. Nanotechnology approaches to drug delivery and imaging. *Journal of Drug Discovery Today*. 2003; 8: 1112-1120.

[23] Mazumder S, Dey R, Mitra MK, Mukherjee S, Das GC. Review: Biofunctionalised quantum dots in biology and medicine. *Journal of Nanomaterials.* 2009:1-17. Doi: 10.1155/2009/815734.

[24] Lakowicz JR. *Principle of fluorescence spectroscopy*. New York: Academic/Plenum Publisher, 2nd edition; 1999.

[25] Gheshlaghi N, Pisheh HS, Karim RM, Unlu H. Interface strain effects on ZnSe/(CdSe) based Type I and ZnSe/CdS Type II core/shell quantum dots. 2016; 102: 152-163. Available from: https://doi.org/10.1016/j.egypro.2016.11.330

[26] Wang CH, Chen CW et al. Surface Plasmon enhanced energy transfer between Type I CdSe/ZnS and Type II CdSe/ZnTe quantum dots. *Journal of Applied Physics Letters*. 96(7). Available from: https://doi.org/10.1063/1.3315876.

[27] Krauss DT, Peterson JJ. Electronic structure and optical transition in colloidal semiconductor nanocrystals. *Colloidal Quantum dots Optoelectronic and Photovoltaics*. 2013: 59-86. Available from: https://doi.org/10.1017/CB09781139022750.004.

[28] Rossetti R, Brus L. Electron-hole recombination emission as a probe of surface-chemistry in aqueous CdS colloids. *Journal of Physical Chemistry*. 1982; 86: 4470-4472.

[29] Gaponenko SV. Introduction to Nanophotonics. Cambridge University Press, Cambridge. 2010.

[30] Yoffe AD. Low-dimensional systems: quantum size effects and electronic properties of semiconductor micro-crystallites (zero-dimensional systems) and some quasi two dimensional systems. *Journal in Advances in Physics*. 1993; 42(2): 173-262. Available from: https://doi.org/10.1080/00018739300101484

[31] Onyia AI, Ikeri HI, Nwobodo AN. Theoretical study of quantum confinement effects on quantum dots using particle in a box model. *Journal of Ovonic Research*. 2018; 14(1): 49-54.

[32] Klimov VI. Nanocrystal quantum dots. Journal of Fundamental Photo-physics to multicolor lasing. 2013; 28: 2014-2020.

[33] Lugovskoy AV, Bray I. Electron relaxation and excitation processes in metal. *Journal of Physics D: Applied physics*. Available from: https://doi.org/10.1088/0022-3727/31/23/001.

[34] Beard MC. Multiple exciton generation in semiconductor quantum dots. *Journal of Physical Chemistry Letters*. 2011; 2(11): 128-1288. Doi: 10.1021/jz200166y.

[35] Miller DAB, Chemla DS, Damen TC, Gossard AC, Wiegmann W, Wood TH, Burrus CA. Bandedge electro-absorption in quantum well structures: the quantum confined stark effect. *Journal of Physical Review letters*. 1984; 53(22): 2173-2176. Available from: https:// ee.stanford.edu/dabm/039.

[36] Arivazhagan V. Quantum confinement effect- an overview. 2013; 1-19. Available from: Shodhganga.inflibnet.ac.in/bitstream/10603/23484/3/03.chapter%201.pdf.

[37] McQuarrie DA, Simon JD. *Physical Chemistry: a molecular approach*. Edwards Brothers; University Science Books. 1997: 77-95.

[38] Neuhauser D, Baer M. A new accurate (time-independent) method for treating three dimensional reactive collisions: The application of optical potentials and projection operators. *Journal of Chemical Physics*. 1998; 92(6). Available from: https://doi.org/10.1063/1.457853.

[39] Dey et al. Confinement energy of quantum dots. Department of Physics. DBCET. Assan Don BOSCO University. 2012. Available from: https://arxiv.org/ftp/papers/1212/1212.2318.

[40] Ekimov AI, Onushchenko AA. Quantum size effects in the optical spectra of semiconductor micro-crystals. *Soviet Physics of Semiconductors*.1982; 16: 775-778.

[41] Michalet X, Pinaud FF, Bentolila LA et al. Quantum dots for live cells, in vivo imaging and diagnostics. *Journal of Sciences*. 2005; 307(5709): 538-544.

[42] Fu A, Gu W, Boussert B et al. Semiconductor quantum rods as single molecule fluorescent biological labels. *Journal of nanomaterial letters.* 2007; 7(1):179-182.

[43] Shen L. Biocompatible polymer/quantum dots hybrid material: Current status and future developments. *Journal of Functional Biomaterials.* 2011; 2: 355-372. Doi: 10.3390/jfb2040355. Available from: https://www.mdpi.com/journal/jfb/.

[44] Mattoussi H, Mauro JM, Goldman ER, Green TM, Anderson GP, Sundar VC, Bawendi MG. Bioconjugation of highly luminescent colloidal CdSe/ZnS quantum dots with an engineered two-domain recombinant protein. *Physica Status Solid B.* 2001; 224(1): 277-283. Available from: https://doi.org/10.1002/1521-3951(200103)224:1

[45] Chan WCW, Nie S. Quantum dot bioconjugates for ultrasensitive nonisotopic detection. *Journal of Sciences*. 1998; 281(5385): 2016-2018.

[46] Lui W, Howarth M, Greytak AB et al. Compact biocompatible quantum dots functionalized for cellular imaging. *Journal of the American Chemical Society*. 2008; 130(4): 1274-1284.

[47] Tomczak N, Janczewski D, Han M, Vancso GJ. Designer polymer- quantum dots architectures. *Progress in Polymer Science*. 2009; 34(5): 393-430. Available from: https://doi.org/10.1016/j.progpolymsci.2008.11.004.

[48] Hezinger AFE, Tebma J, Gopferich A. Polymer coating of quantum dots – a powerful tool toward diagnostics and sensorics. *European Journal of Pharmaceutics and Biopharmaceutics*. 2008; 68(1): 138-152. http://doi.org/10.1016/j.ejpb.2007.05.013.

[49] Joglekar SS, Ghoplap HM, Alegaonkar PS, Kale AA. The interaction between CdTe quantum dots and proteins: understanding nano-bio interface. *AIMS Material Science.* 2017; 4(1): 209-222. Doi: 10.3934/matersci.2017.1.209.

[50] Wu F, Lewis JW, Kliger DS et al. Unusual excitation intensity dependence of fluorescence of CdTe nanoparticles. *Journal of Physical Chemistry*. 2003; 118: 12-16.

[51] Leckband D. Measuring the forces that control protein interactions. *Annual reviews of biophysics and biomolecular structure.* 2000; 29: 1-26. Doi: 10.1146/annurev.biophys.29.1.1

[52] Xiao Q, Huang S, Qi ZD, Zhou B, He ZK, Liu Y. Conformation, thermodynamics and stoichiometry of HAS adsorbed to colloidal CdSe/ZnS quantum dots. *Bba-Proteins Proteom*. 2008; 1784: 1020-1027.

[53] Poderys V, Matulionyte M, Selskis A, Rotomskis R. Interaction of water-soluble CdTe quantum dots with bovine serum albumin. *Nanoscale Research Letters*. 2011; 6(9): 1-6. Available from: http://www.nanoscalereslett.com/content/6/1/9.

[54] Hu DH, Wu HM, Liang JG, Han HY. Study on the interaction between CdSe quantum dots and hemoglobin. *Spectrochimica Acta Part A*. 2007; 69: 830-834. Doi: 10.106/j.saa.2007.05.036.

[55] Hasani M, Rezae A. Spectrophotometric study of the charge- transfer complexes of iodine with antipyrine in organic solvent. Spectrochimica Acta Part A: *Molecular and biomolecule spectroscopy*. 2006; 65(5): 1093-1097. https://dio.org/10.1016/j.saa.2006.02.009

[56] Liu MC, Shi GY, Zhang L, Cheng YX, Jin LT. Quantum dots modified electrode and its application in electroanalysis of hemoglobin. *Electrochemistry communications*. 2006; 8(2): 305-310. Available from: https://doi.org/10.106/j.elecom.2005.11.026.

[57] Xiao Q, Huang S, Qi ZD, Zhou B, He ZK, Liu Y. Conformation, thermodynamics and stoichiometry of HAS adsorbed to colloidal CdSe/ZnS quantum dots. *Bba-Proteins Proteom*. 2008; 1784: 1020-1027.

[58] Dzagli MM, Canpean V, Losin M, Mohou MA, Astilean S. Study of the interaction between CdSe/ZnS core-shell quantum dots and bovine serum albumin by spectroscopic techniques. *Journal of Photochemistry and Photobiology A: Chemistry*. 2010; 215(1): 118-122. Available from: https://doi.org/10.1016/j.jphotochem.2010.08.008

[59] Maiti A, Bhattacharyya S. Review: Quantum dots and application in medical science. *International Journal of Chemistry and Chemical Engineering*. 2013; 3(2): 37-42. Available from: https://www.ripublication.com.

[60] Zimmer JP, Kim SW, Ohnishi S, Tanaka E, Frangioni JV, Bawendi MG. Size series of small Indium Arsenide-Zinc selenide core-shell nanocrystals and their application to in vivo imaging. *Journal of American Chemical Society*. 2006; 128: 2526-2527. https://doi.org/10.1012/ja0579816.

[61] Costa-Fernandez JM, Pereiro R, Sanz-Medel A. The use of luminescent quantum dots for optical sensing. *TrAC Trends in Analytical Chemistry*. 2006; 25(3): 207-218. Available from: Doi: 10.1016/j.trac.2005.07.008

[62] Derfus AM, Chan WCW, Bhatia SN. Intercellular delivery of quantum dots for live cell labelling and organelle tracking. Advanced material. 2004; 16: 961-966.

[63] Kwaambwa HM, Hellsing MS, Rennie AR, Barker R. The interaction of Molinga Oleifera seed protein with a mineral surface and the influence of surfactants. *Journal of colloid and interface Science.* Available from: https://dx.doi.org/10.106/j.jcis.2015.02.033

[64] Aho IM, Legasi JE. A new water treatment system using *Moringa oleifera* seed. *American journal of scientific and industrial research*. 2012; 3(6): 487-492. Doi: 10.5251/ajsir.2012.3.6.487.492.

[65] Bodlund I. Coagulant protein from plant materials: Potential water treatment agent. School of Biotechnology, Royal Institute of technology (KTH), AlbaNova University Center, Sweden 2013.

[66] Ali EN, Muyibi SA, Salleh HM, Salleh MRM, Alam MZ. *Moringa oleifera* seeds as natural coagulant for water treatment. *Thirteenth International Water Technology Conference.* 2009; 13:163-168.

[67] Eilert U. Antibiotic principles of seeds of *Moringa oleifera*. *Indian Medicinal Journal*. 1978; 38(235): 1013-1016.

[68] Ndabigengesere A, Narasiah KS, Talbot BG. Active agents and mechanism coagulation of turbid waters using *Moringa oleifera. Water Resource.* 1995; 29: 703-710.

[69] Kwaambwa HM, Maikokera R. A fluorescence spectroscopic study of a coagulating protein extracted from *Moringa oleifera* seeds. 2007; 60(2): 213-220. Available from: https://doi.org/10.1016/j.colsurfb.2007.06.015.

[70] Ndabigengesere A, Narasiah KS. Quality of water treated by coagulation using *Moringa oleifera* seeds. *Water Resources*. 1998; 32: 781-791.

[71] Kwaambwa HM, Maikokera R, Infrared and circular dichroism spectroscopic characterization of secondary structure components of a water treatment coagulant protein extracted from *Moringa oleifera* seeds. *Colloids and Surfaces B: Biointerfaces*. 2008; 64: 118-125. Available from: doi: 10.1016/j.colsurfb.2008.01.014

[72] Olanrewaju RF, Muyibi SA, Salawudeen TO, Aibinu AM. An intelligent modelling of coagulant dosing system for water treatment plants based on artificial neural network. *Australia basic applied science.* 2012; 6: 93-99.

[73] Muyibi SA, Okuofu CA, Coagulation of low turbidity surface waters with *Moringa oleifera* seeds. *International Journal of Environmental studies*. 1995; 48(3):263-273.

[74] Arku AY, Musa SM, Mofoke ALE. Characterization and standardization of crude *Moringa oleifera* seeds for wastewater treatment. *Journal of applied phytotechnology Environment San.* 2012; 1: 67-74.

[75] Obuseng V, Nareetsile F, Kwaambwa HM. A study of the removal of heavy metals from aqueous solutions by *Moringa oleifera* seeds and amine-based ligand 1,4-bis[N,N-bis(2-picoyl)amino]butane. *Analytica Chimica Acta.* 2012; 730: 87-92. Doi: 10.1016/j.ac.2012.01.054.

[76] Agbahoungbata MY, Fatombi JK. Removal of reactive dyes from their aqueous solutions using *Moringa oleifera* seeds and *Grewia venusta* peel. *Desalination and water treatment.* 2016; 57(47): 22609-22617.

[77] Santos AFS, Paiva PMG, Teixeira JA, Brito AG, Coelho LCBB, Nogueira RB. Coagulant properties of *Moringa oleifera* protein preparation: application to humic acids removal. *Environmental Technology*. 2012; 33(1-3): 69-75.

[78] Kwaambwa HM, Maikokera R, Nermark FM. Surface activity interaction in aqueous solution of anionic surfactants with a water treatment protein from *Moringa oleifera* seeds. *Green and Sustainable Chemistry*. 2015; 5: 31-38. Available from: DOI: 10.4236/gsc.2015.51005

[79] Pavankumar AR, Singh L. Identification of *Moringa oleifera* protein responsible for the decolorization and pesticide removal from drinking water and industrial effluent- an in silico and in situ evaluation. *Journal of Chemistry Technology and Biotechnology*. 2014; 90: 1521-1526. Doi: 10.1002/jctb.4468.

[80] Maikokera R, Kwaambwa HM, Use of viscosity to probe the interaction of anionic surfactants with a coagulant protein from *Moringa oleifera* seeds. *Research letter in Physical Chemistry*. 2009; ID 927329; doi: 10.1155/2009/927329.

[81] Deo P, Jockusch S, Ottaviani MF, Moscatelli A, Turro NJ, Somasundaran P. Interactions of hydrophobically modified polyelectrolytes with surfactants of the same charge. *Langmuir*. 2003; 19(26); 10747-10752.

[82] Kwaambwa HM, Nermark FM. Interactions in aqueous solution of zwitterionic surfactant with treatment Protein from *Moringa oleifera* seeds studied by surface tension and ultrasonic velocity measurements. *Green and Sustainable Chemistry*. 2013; 3: 135-140. Available from: http://dx.doi.org/10.4236/gsc.2013.34016.

[83] Kwaambwa HM, Maikokera R. Air-water interface interaction of anionic, cationic and non-ionic surfactants with a coagulant protein extracted from *Moringa oleifera* seeds studied using surface tension probe. *Water Resources*. 2007; 33: 583-588.

[84] Gupta DK, Verma M, Sharma KB, Saxena NS. Synthesis, characterization and optical properties of CdSe/CdS and CdSe/ZnS core-shell nanoparticles. *Indian Journal of Pure and Applied Physics.* 2017; 55: 113-121.

[85] Kathiresan R, Gopalakrishnan S, Kolandaivel P. Interaction and bioconjugation of CdSe/ZnS core/shell quantum dots with maltose binding protein. *Computational and Theoretical Chemistry*. 2017; 1101:96-101. https://dx.doi.org/10.1016/j.comptc.2016.12.038.

[86] Yu WW, Qu LH, Guo XG, Peng XG. Experimental determination of the extinction coefficient of CdTe, CdSe and CdS Nanocrystals. *Journal of Chemistry of Materials*. 2003; 15(14): 2854-2860. Doi: 10.1021/cm034081k

[87] Tauc J. Amorphous and Liquid semiconductors. Plenum press, London and New York. Available from: http://dx.doi.org/10.1007/978-1-4615-8705-7.

[88] Amiri GR, Fatahian S, Mahmoudi S. Preparation and Optical properties assessment of CdSe QDs. *Journal of Material Sciences and Application.* 2013; 4:134-137. Available from: http://dx.doi.org/10.4236/msa.2013.42015.

[89] Li S, Wang YZ, Jiang JG, Dong SJ. PH-dependent protein conformation changes in albumin: gold nanoparticles bioconjugates. *Journal of Spectroscopic Study Langmuir*. 2007; 23: 2714-2720.

[90] Hiratsuka T. Conformational changes in the 23-kilodalton NH2-terminal peptide segment of myosin ATPase associated with ATP hydrolysis. Journal of Biological Chemistry. 1990; 265: 18786-18790.

[91] Schmidts S, Behra M, Uhlig K, Madaboosi N, Hartmann L, Duschl C, Volodkin D. Mesoporous Protein particles through colloidal $CaCO_3$ templates. Journal of Advanced functional materials. 2013; 23(1): 116-123.

[92] Slowing II, Trewyn BG, Lin VSY. Mesoporous silica nanoparticles for intracellular delivery of membrane-impermeable proteins. Journal of American Chemical Society. 2007; 129(28): 8845-8849. Doi: 10.1021/ja0719780.

[93] Dzagli MM, Canpean V, Iosin M. Study of the interaction between CdSe/ZnS core-shell quantum dots and bovine serum albumin by spectroscopic techniques. *Journal of Photochemistry and Photobiology A: Chemistry*. 2010; 215: 118-122. Doi: 10.1016/j.jphotochem.2010.08.008.

[94] Pan BF, Gao F, Ao LM. Investigation of interaction between dendrimer-coated magnetite nanoparticles and bovine serum albumin. *Journal of magnetite materials*. 2005; 293: 252-258.

[95] Okamoto K, Vyawahare S, Sherer A. Surface-Plasmon enhanced bright emission from CdSe quantum dot nanocrystals. Journal of the Optical Society of America B. 2006; 23(8): 1674-1678.

[96] Lai L, Lin C, Xu ZQ, Han XL, Tian FF, Mei P, Li DW, Ge YS, Jiang FL, Zhang YZ, Lui YI. Spectroscopic studies on the interaction between CdTe quantum dots coated with different ligands and human Serum albumin. *Journal of Spectrochimica Acta part A: Molecular and Biomolecular Spectroscopy.* 2012; 97: 366-376. Available from: http://dx.doi.org/10.1016/j.saa.2012.06.025.

[97] Yan H, Wu G, Dai G et al. Interaction mechanisms of ionic liquid [Cnmim] Br [n=4,6,8,10] with bovine serum albumin. *Journal of Luminescence*. 2012; 132(3): 622-628.

[98] Hu YJ, Liu Y, Zhang LX, Zhao RM, Qu SS. Studies of interaction between colchicine and bovine serum albumin by fluorescence quenching method. *Journal of Molecular Structure*. 2005; 750: 174-178.

[99] Hasani M, Rezaei A. Spectrophotometric study of the charge-transfer complexes of iodine with antipyrine in organic solvent. Journal of Spectrochimica Acta. Part A. Molecular and biomolecular Spectroscopy. 2006; 65(5): 1093-1097. Doi: 10.1016/J.saa.2006.02.009.

[100] Liu P, Liu Y, Wang Q. Studies on the interaction of CdTe QDs with bovine serum albumin. *Journal of Chemical technology and biotechnology*. 2012; 87: 1670-1675. Doi: 10.1002/jctb.3815.

[101] Tian J, Liu J, He W, Hu Z, Yao X, Chen X. Probing the binding of scutellarin to human serum albumin by circular dichroism, fluorescence spectroscopy, FTIR and molecular modeling method. *Journal of Bio-macromolecules*. 2004; 5(5): 1956-1961.

[102] Zheng C, Wang H, Xu W, Xu C, Liang J, Han H. Study on the interaction between histidine-capped Au nanoclusters and bovine serum albumin with spectroscopic technique. *Journal of Spectrochimica Acta-Part A: Molecular and Biochemistry*. 2014; 118: 897-902.

[103] Fu Y, Guan E, Liang J, Ren G, Chen L. Probing the effect of Ag_2S quantum dots on human serum albumin using spectral techniques. *Journal of Nanomaterials*. 2017; 1-7. Available from: https://doi.org/10.1155/2017/7209489.

[104] Dave H, Troullier A, Veteau MI, Dunach G, Padros LE. Secondary structure components and properties of melibiose permease from *Escherichia coli*: A Fourier transform infrared spectroscopy analysis. *Journal of Biophysical*. 2000; 79(2): 747-755. Available from: https://doi.org/10.1016/S0006-3495(00)76332-6.

[105] Cabiaux V, Oberg KA, Pancoska P, Walz T, Agre P, Engel A. Secondary structures comparison of aquaporin-1 and bacteriorhodopsin: A Fourier transform infrared spectroscopy study of two dimensional membrane crystals. *Journal of Biophysical*. 1997; 73(1): 406-417. Available from: https://doi.org/10.1016/S0006-3495(97)78080-9

APPENDICES

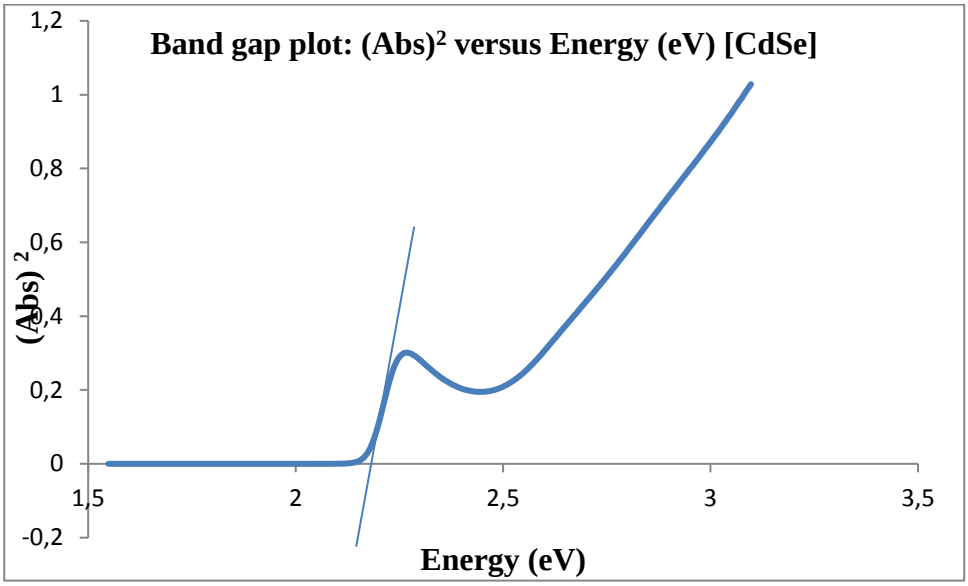

Figure 17: The Tauc plot of direct band gap, $(Abs)^2$ versus Energy (eV) of CdSe QDs.

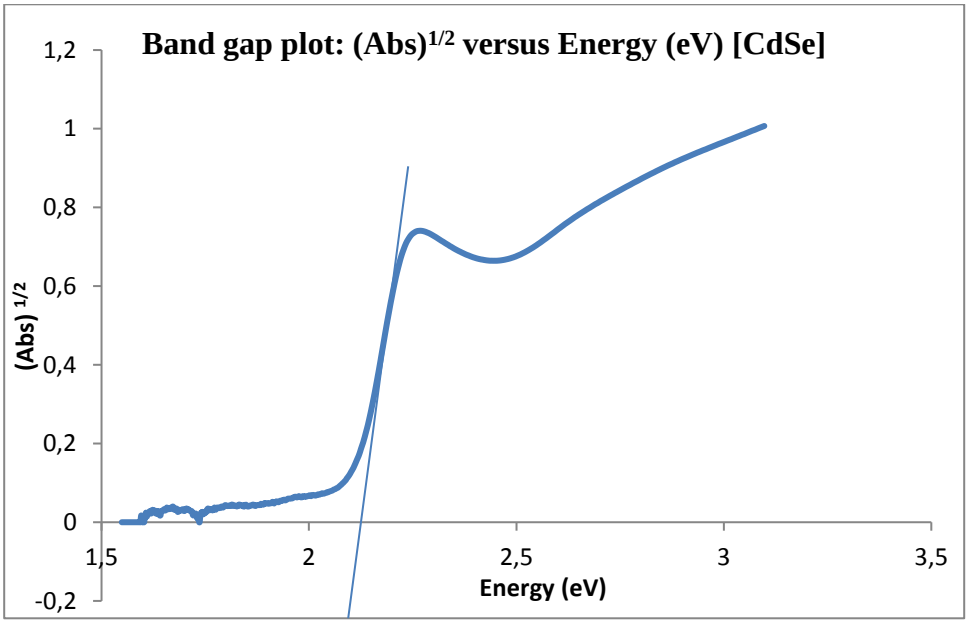

Figure 18: The Tauc plot of indirect band gap, $(Abs)^{1/2}$ versus Energy (eV) of CdSe QDs.

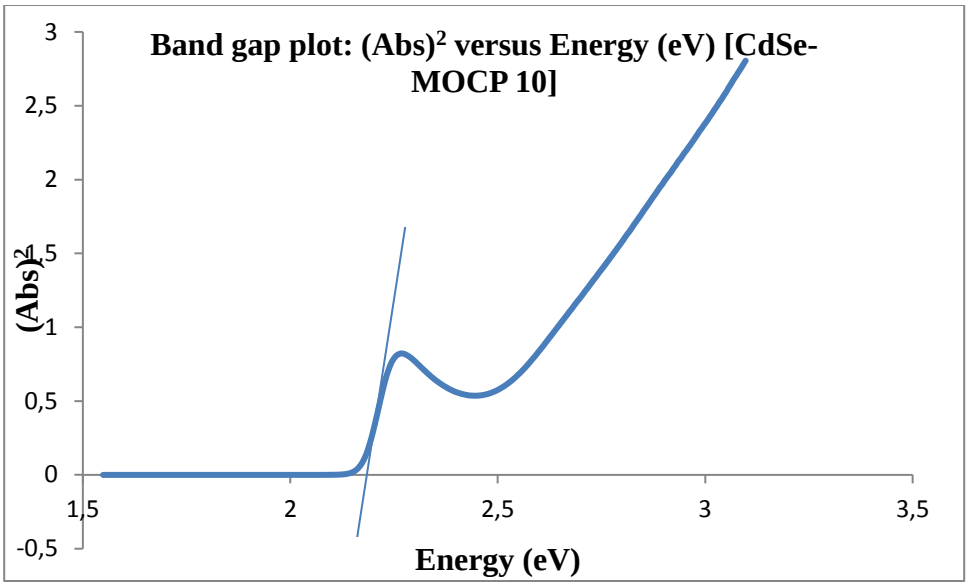

Figure 19: The Tauc plot of direct band gap, $(Abs)^2$ versus Energy (eV) of CdSe-MOCP (10 mg/mL).

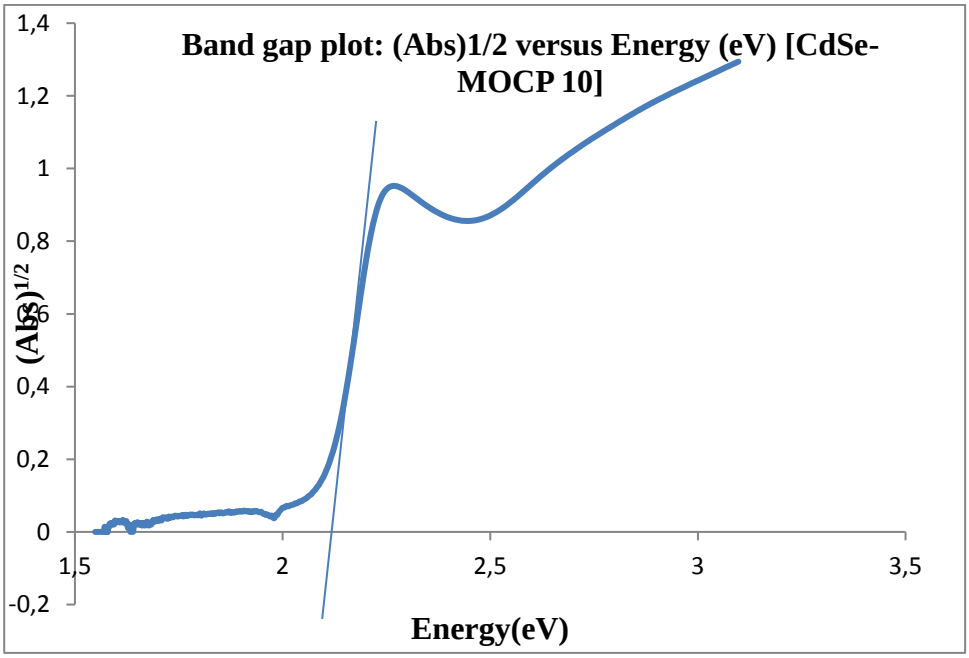

Figure 20: The Tauc plot of indirect band gap, $(Abs)^{1/2}$ versus Energy (eV) of CdSe-MOCP (10 mg/mL).

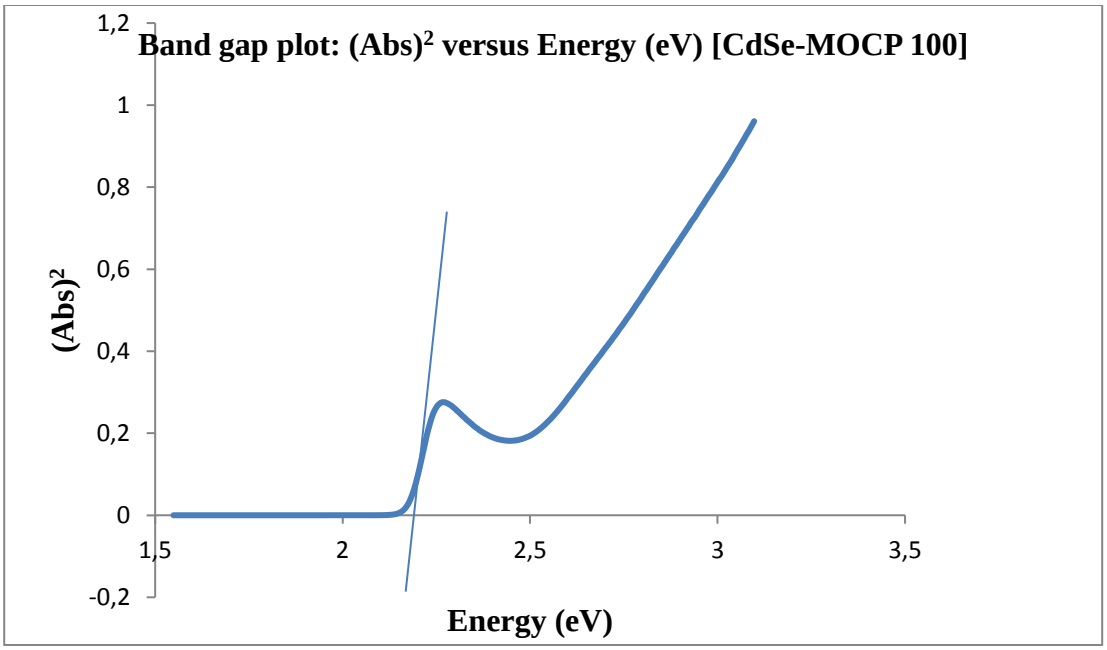

Figure 21: The Tauc plot of direct band gap, $(Abs)^2$ versus Energy (eV) of CdSe-MOCP (100 mg/mL).

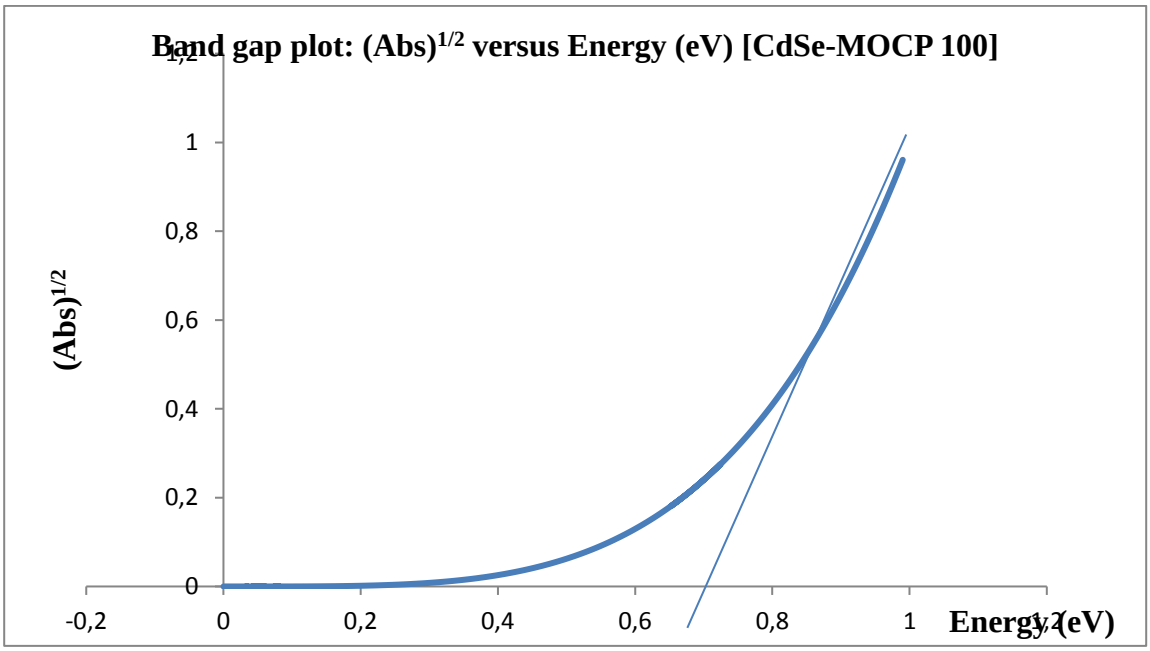

Figure 22: The Tauc plot of indirect band gap, $(Abs)^{1/2}$ versus Energy (eV) of CdSe-MOCP (100 mg/mL).

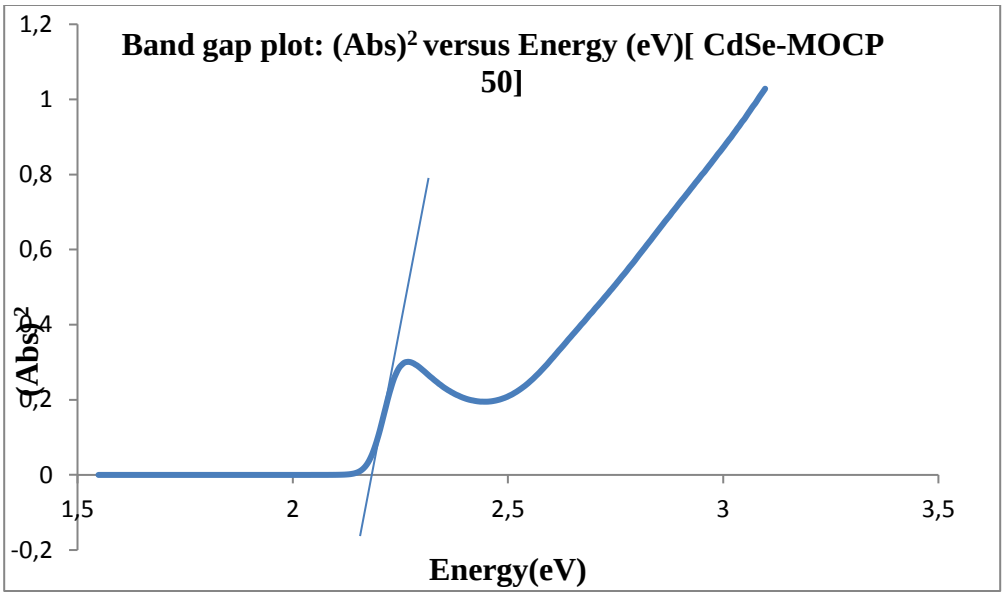

Figure 23: The Tauc plot of direct band gap, $(Abs)^2$ versus Energy (eV) of CdSe-MOCP (50 mg/mL).

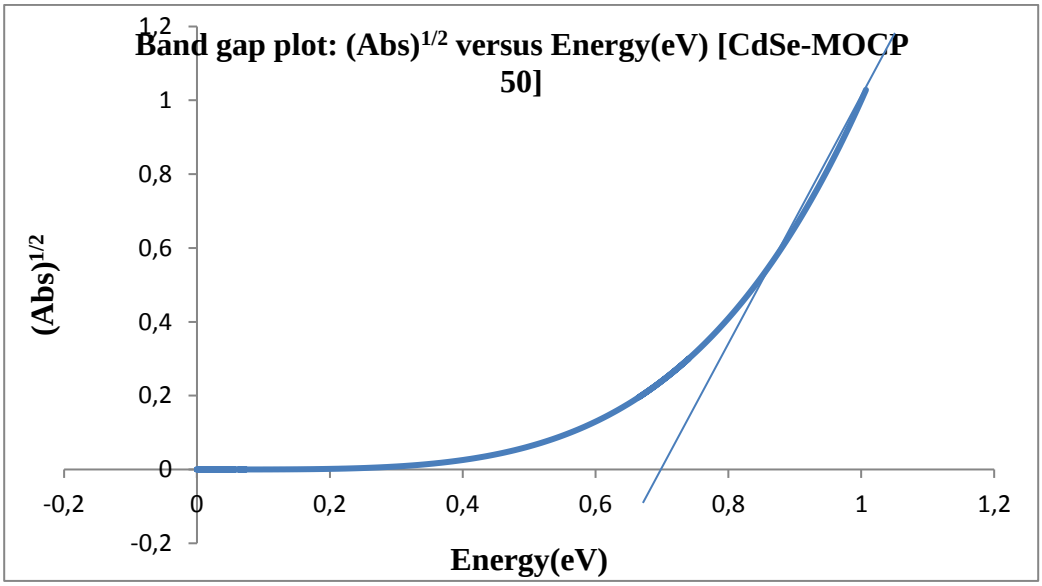

Figure 24: The Tauc plot of indirect band gap, $(Abs)^{1/2}$ versus Energy (eV) of CdSe-MOCP (100 mg/mL).

Table 8: BET analysis Isotherm linear plot (Moringa Adsorption).

Relative Pressure (P/Po)	**Quantity Adsorbed (cm^3/g STP)**
0.057050800	0.888507971
0.099649602	1.215470488
0.149644114	1.564257622
0.199514608	1.867160519
0.249443844	2.111186746
0.299386124	2.284648505
0.993571648	15.88959158

Table 9: BET MOCP Surface Area plot

Relative Pressure (P/Po)	**$P/[V_a(P_0-P)]$**
0.057050800	0.068095
0.099649602	0.091058
0.149644114	0.112500
0.199514608	0.133487
0.249443844	0.157421
0.299386124	0.187040

Table 10: Fluorescence spectra intensities of CdSe-MOCPn System

[CdSe-MOCP mg/mL]	**FL intensity (F)**	**Relative FL(F_0/F)**
0	F_0= 683.65	
10	620.93	1.10
25	412.38	1.66
50	286.52	2.39
80	188.07	3.64
100	158.11	4.32

Table 11: Scatchard relation plot for determination of thermodynamic potentials at T=298.15

CdSe-MOCP$_n$ (Mx10^{-6})	**log [Q]**	**FL intensity (F)**	**(F_0-F)/F**	**log[(F_0-F)/F]**
0.769	-6.11	620.93	0.10	-1.00
1.92	-5.72	412.38	0.66	-0.18
3.85	-5.41	286.52	1.39	0.14
6.15	-5.21	188.07	2.64	0.42
7.69	-5.11	158.11	3.32	0.52

Table 12: Scatchard relation plot for determination of thermodynamic potentials at T=313.15

CdSe-MOCP$_n$ (Mx10^{-6})	**log [Q]**	**FL intensity (F)**	**(F_0-F)/F**	**log[(F_0-F)/F]**
0.769	-6.11	600.84	0.05	-1.30
1.92	-5.72	504.70	0.25	-0.60
3.85	-5.41	216.80	1.91	0.28
6.15	-5.21	156.94	3.02	0.48
7.69	-5.11	124.43	4.07	0.61